AWARD NUMBER: W81XWH-14-1-0482

TITLE: A Combination Tissue Engineering Strategy for Schwann Cell-Induced Spinal Cord Repair

PRINCIPAL INVESTIGATOR: Treena Arinzeh

CONTRACTING ORGANIZATION: New Jersey Institute of Technology
Neward, NJ 07102

REPORT DATE: October 2015

TYPE OF REPORT: Annual

PREPARED FOR: U.S. Army Medical Research and Materiel Command
Fort Detrick, Maryland 21702-5012

REPORT DOCUMENTATION PAGE

Form Approved
OMB No. 0704-0188

1. REPORT DATE	2. REPORT TYPE	3. DATES COVERED
October 2015	Annual	30 Sep 2014 – 29 Sep 2015

4. TITLE AND SUBTITLE

A Combination Tissue Engineering Strategy for Schwann Cell-Induced Spinal Cord Repair

5a. CONTRACT NUMBER

5b. GRANT NUMBER
W81XWH-14-1-0482

5c. PROGRAM ELEMENT NUMBER

6. AUTHOR(S)
Treena Arinzeh
Mary Bunge
Mesut Sahin

E-Mail: arinzeh@njit.edu

5d. PROJECT NUMBER

5e. TASK NUMBER

5f. WORK UNIT NUMBER

7. PERFORMING ORGANIZATION NAME(S) AND ADDRESS(ES)
New Jersey Institute of Technology
323 Martin Luther King Blvd.
Newark, NJ 07102

8. PERFORMING ORGANIZATION REPORT NUMBER

9. SPONSORING / MONITORING AGENCY NAME(S) AND ADDRESS(ES)

U.S. Army Medical Research and Materiel Command
Fort Detrick, Maryland 21702-5012

10. SPONSOR/MONITOR'S ACRONYM(S)

11. SPONSOR/MONITOR'S REPORT NUMBER(S)

12. DISTRIBUTION / AVAILABILITY STATEMENT

Approved for Public Release; Distribution Unlimited

13. SUPPLEMENTARY NOTES

14. ABSTRACT

This study proposes a novel tissue engineering strategy utilizing electroactive conduits, neurotrophins and Schwann cells (SCs) to treat spinal cord injuries. The conduits have piezoelectric activity, which means they are able to generate electrical activity in response to minute deformations. The conduits containing SCs and releasing neurotrophins will promote axonal regeneration in the injured site and into the caudal cord to improve functional recovery. During this first year of funding, hollow versus fiber filled conduits containing SCs were evaluated in completely transected spinal cords for promoting axonal regeneration. Conduits also were coated with or without Matrigel, a basement membrane protein matrix, to evaluate if Matrigel was necessary for SC survival and axonal growth. More axons and SCs were observed in the fiber-filled conduits containing Matrigel. The fibers enabled contact guidance for directed axon regeneration along the rostral/caudal axis regardless of the use of Matrigel. In vitro findings also complimented in vivo findings where greater neurite extension was determined on SC containing aligned fibers with or without Matrigel coating.

15. SUBJECT TERMS

Polyvinylidenefluoride-trifluoroethylene (PVDF-TrFE), piezoelectric, aligned, electrospun, spinal cord repair, Schwann cells, Matrigel, brain-derived growth factor (BDNF), neurotrophin-3 (NT3), poly(ethylene oxide) (PEO), controlled release, functional recovery.

16. SECURITY CLASSIFICATION OF:			17. LIMITATION OF ABSTRACT	18. NUMBER OF PAGES	19a. NAME OF RESPONSIBLE PERSON
a. REPORT	b. ABSTRACT	c. THIS PAGE			USAMRMC
Unclassified	Unclassified	Unclassified	Unclassified	41	19b. TELEPHONE NUMBER *(include area code)*

Table of Contents

Page

1. INTRODUCTION

This proposal seeks to improve axonal regeneration and functional recovery in spinal cord injury (SCI) by utilizing a piezoelectric conduit containing Schwann cells (SCs) that provide both physical and neurotrophic cues and neurotrophin release caudal to the injury site. Piezoelectric materials provide electrical activity in response to minute deformation. This project investigates the design of the piezoelectric conduits containing SCs by examining hollow versus fiber-filled conduits for promoting axonal growth. This project also determines if axons extend into the caudal spinal cord parenchyma following the controlled release of neurotrophins at and below the SC conduit. The conduit is designed to release two neurotrophins and additional neurotrophin delivery is provided caudal to the injury site to promote axonal regeneration into, through and out of the SC conduit and into the caudal cord to improve functional recovery. Experiments are performed both *in vitro* and *in vivo* to assess axonal regeneration.

2. KEYWORDS

Polyvinylidenefluoride-trifluoroethylene (PVDF-TrFE), piezoelectric, aligned, electrospun, spinal cord repair, Schwann cells, Matrigel, brain-derived growth factor (BDNF), neurotrophin-3 (NT3), poly(ethylene oxide) (PEO), controlled release, functional recovery.

3. ACCOMPLISHMENTS

What were the major goals of the project?

1. ***Evaluate piezoelectric conduits with Schwann cells (SC)s for axonal growth with or without Matrigel.***
    a. Acuro Approval – Period: 0 months, 100% completed
    b. Fiber fabrication, materials characterization, and piezoelectric characterization, Period: 1-12 months, 90% completed
    c. *In vitro* characterization of SC survival, myelination and neurite extension on piezoelectric fibers, Period: 1-12 months, 100% completed
    d. Piezoelectric conduits will be evaluated in a complete transection model, Period:1-12 months, 95% completed
2. ***Determine if axons extend into the caudal spinal parenchyma following the controlled release of neurotrophins at and below the SC conduit and improve functional recovery.***
    a. *In vitro* characterization of the controlled release of neurotrophin-3 (NT3) and brain-derived growth factor (BDNF) from the fibrous piezoelectric scaffolds will be evaluated for neurite extension and SC survival, Period: 13-24 months, 0% completed.
    b. *In vitro* characterization of the controlled release of NT3 and BDNF from the PEO hydrogel will be evaluated and DRG neurite outgrowth measured, Period: 13-24 months, 0% completed.
    c. A pilot *in vivo* study will be performed to determine axon growth into, through and out of the SC- piezoelectric conduit with NT3 and BDNF release, Period: 19-24 months, 0% completed.
    d. The full in vivo study will be performed to determine axon growth into, through and out of the SC- piezoelectric conduit with NT3 and BDNF release, Period: 25-36 months, 0%

What was accomplished under these goals?

1. **Major Activities**
    The major activities accomplished during this period were:
    a. Fiber fabrication, materials characterization and piezoelectric characterization were performed.

b. *In vitro* studies of SC growth and SC co-cultures with dorsal root ganglion (DRG) to evaluate neurite extension on piezoelectric scaffolds were performed.
c. *In vivo* studies using piezoelectric conduits filled with aligned fibers with or without matrigel containing SCs were performed in the rat complete transection model.

2. Specific Objectives

The specific objectives were as follows:

a. The piezoelectric fibrous scaffolds were fabricated, characterized for chemistry and for electrical output in vitro in wet conditions using the microelectrode arrays.
b. SC growth on piezoelectric scaffolds and SC co-cultures with DRG using different SC seeding densities was performed on the piezoelectric scaffolds to evaluate neurite extension.
c. Piezoelectric conduits filled with aligned fibers containing SCs with or without matrigel were evaluated in the complete transection model in the rat.

3. Significant Results

3.1. **Piezoelectric scaffold fabrication and characterization *in vitro***

Fabrication of piezoelectric scaffolds was performed by electrospinning polyvinylidine fluoride-trifluoroethylene (PVDF-TrFE). 15% (w/v) of PVDF-TrFE (65/35) (Solvay Solexis, Inc.) was dissolved in methyl ethyl ketone (MEK) and electrospun using a fast-rotating drum to collect aligned fibers. Fiber size, alignment and interfiber spacing was measured using scanning electron microscope (SEM) images and Image J software. Fiber size was 548±139 nm having uniform fiber morphology, interfiber spacing was 4.13±1.27μm, and the degree of alignment was 89.3±9.9% for 15% PVDF-TrFE scaffolds

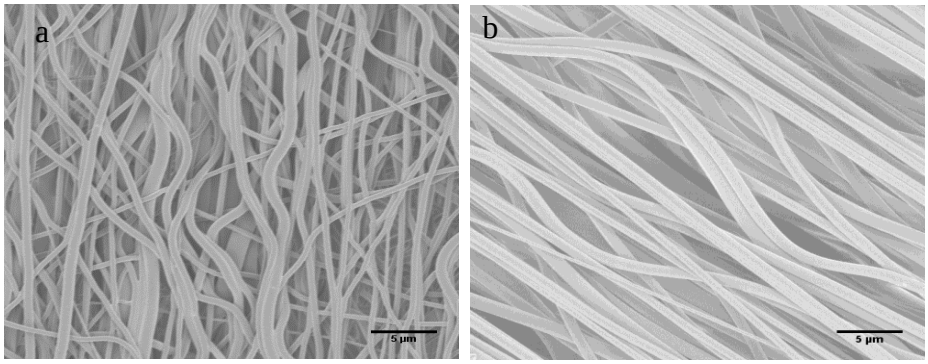

Figure 1. SEM image of aligned PVDF-TrFE using a) 15% (w/v) and b) 20% (w/v).of PVDF-TrFE dissolved in MEK.

(Figure 1.a). Fiber diameter was 1.14 ± 0.37 μm, interfiber spacing was 8.89±3.79 μm and the alignment was 92.8%±7.0% for the 20% PVDF-TrFE scaffolds (Figure 1.b.). Porosity was measured by the density difference between the scaffold and the unprocessed material. The porosity was 87.1±1.5% and 84.3±1.7% for 15 and 20% PVDF-TrFE scaffolds, respectively. The 20% PVDF-TrFE scaffolds were prepared in order to increase interfiber spacing to support cell infiltration. The fibers prepared using the 20% PVDF-TrFE formulation was used inside of the conduit for evaluation in the rat complete transection model.

The above mentioned scaffolds were all annealed to increase the piezoelectric crystal phase or β-phase content. We have also prepared other formulations, PVDF-TrFE containing 1% PEO (PVDF-TrFE-PEO) for growth factor release studies in Aim 2/Year 2 studies and unannealed PVDF-TrFE for comparison. We characterized the presence of the β-phase by fourier transform infrared spectroscopy (FTIR) and x-ray diffraction (XRD) as shown in Figures 2 and 3, respectively. FTIR spectra showed main peaks for PVDF-TrFE β phase at 1430, 1399, 1286, 1179, 881, 844, 506 and 471 cm^{-1}. The annealed scaffolds showed an increase in peak intensity at 1286 cm^{-1} compared to unannealed scaffolds. For XRD, the spectra showed a peak at 20.1° corresponding to the β phase, and shoulder at 18.6° corresponding to the α phase. The annealing process increased the intensity of the peak for β phase, and removed the shoulder for α phase which indicates that the annealing process increased the β phase in the fibers and decreased the α presenting in the fibers. Interesting, the addition of the PEO to PVDF-TrFE did not affect the presence of the β-phase, which appeared comparable to the unannealed PVDF-TrFE. The amount of the β-phase content determined using FTIR was 64±6% for unnannealed PVDF-TrFE, 67±3% for PVDF-TrFE containing PEO, and 77±1% for annealed PVDF-TrFE, where the annealed PVDF-TrFE had the highest β-phase, or piezoelectric phase, content. The percent crystallinity was measured using Differential Scanning Calorimetry (DSC). 55±2% for unnannealed PVDF-TrFE, 59±4% for PVDF-TrFE containing PEO, and 68±3% for annealed PVDF-TrFE. The crystallinity was significantly higher for the annealed material.

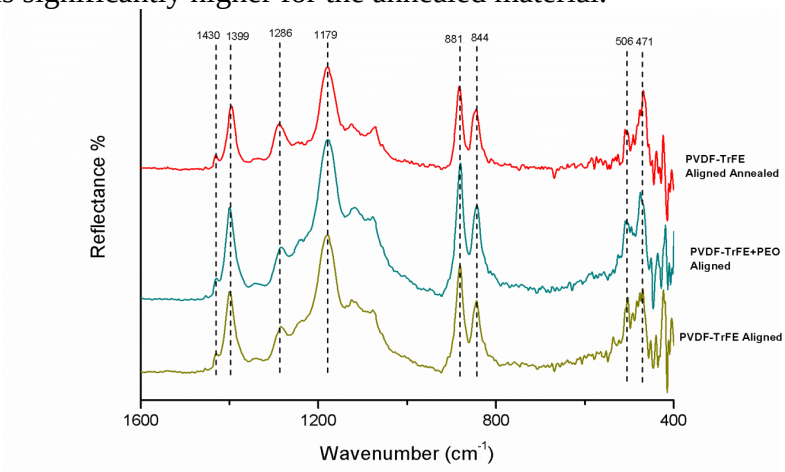

Figure 2. FTIR spectra of PVDF-TrFE scaffolds.

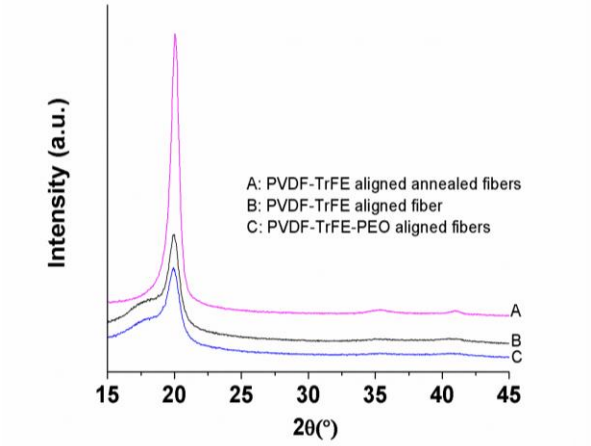

Figure 3: XRD spectra of PVDF-TrFE scaffolds.

Piezoelectric activity of the aligned scaffold in dry conditions was characterized by subjecting the fibers to cyclic compression testing (Instron 3340) at a frequency ranging from 1-10 Hz and 10-30% deformation in dry conditions. The range of electrical output and electric fields are shown in Table 1. The results show that at 1 Hz, 10% deformation, which is physiological loading conditions, the electric field is 0.326 V/mm or 326 mV/mm, which is consistent with electric fields used to stimulate neurite outgrowth.

Table 1: Electric output of aligned PVDF-TrFE scaffolds tested in dry conditions at different frequencies and deformations in compression.

Oscillate Frequency (Hz)	% Deformation	Voltage output(V)	Electric Field (V/mm)
1	10%	0.078	0.326
	20%	0.42	1.75
	30%	2.26	9.42
5	10%	2.86	11.92
	20%	6.31	26.29
	30%	8.75	36.46
10	10%	8.75	36.46

Piezoelectric activity measurements of the PVDF-TrFE scaffolds in wet conditions *in vitro* and in the *in vivo* model. Piezeoelectric measurements *in vitro* in wet conditions were conducted using the microelectrode array setup that will be used in the *in vivo* characterization model. Studies *in vitro* in wet conditions needed to be performed prior to *in vivo* characterization in order to characterize the expected electrical output *in vivo*.

A multi-contact electrode array was custom-made by NeuroNexus with 50um contact diameters and 300um pitch in a 4x8 configuration. The array substrate is a 12um polyimide and therefore very flexible. The contacts were made of gold and coated with PEDOT to reduce their impedances Dr. Sahin's laboratory at the New Jersey Institute of Technology. PVDF-TrFE scaffolds were tested in saline in a Faraday cage to block any electromagnetic interference: 1. Control fibers (polycaprolactone, PCL) which is a non-piezoelectric material and 2. Aligned fibers of PVDF-TrFE. The fiber scaffolds were cut into about 2x2mm pads and placed over the electrode array in saline covering half of the contacts for comparison. A piece of glass slide was placed on the fiber scaffold to hold it down. For this preliminary testing, a cyclic force was applied manually on the glass slide with a Q-tip at a constant pace of about 2-3Hz. The AC signals generated in medium were amplified by a 32-channel wireless amplifier (gain=800, band-pass=0.8Hz-3kHz, TBSI Systems) connected to the contacts of the array and sampled into the computer at 10 ksamples/s.

The peak-to-peak amplitude of the streaming potentials after dividing by the amplifier's gain is around 100uV. The frequency spectra of the signals recorded via multipole contacts are shown in Figure 4 (each color represents a channel). The FFT plots show a large peak at the frequency of the mechanical perturbation (2-3Hz) in both samples, however, there is much more power in the PVDF-TrEE sample overall. The frequency spectra for the aligned-fibers contain signal power above and beyond the first and second harmonics of the mechanical stimulus, unlike the control sample on the right. This finding shows that the

aligned PVDF-TrFE fibers generate field potentials that show up at higher harmonics of the mechanical stimulus. There may be components also at the frequency of the mechanical stimulus, however, these are difficult to delineate from the electrode half-cell potential.

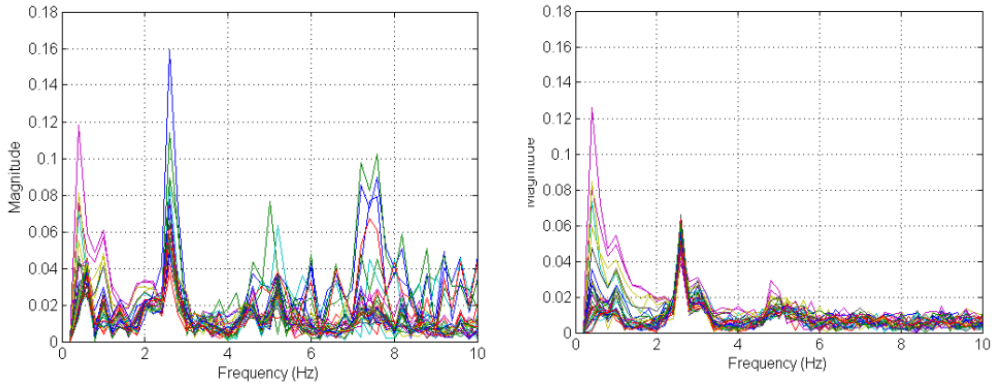

Figure 4. Streaming potentials measured with aligned PVDF-TrFE fibers (left plot) and the control PCL fibers (right plot). There is more power generated in the PVDF-TrFE fibers.

A mechanical setup was built to induce micrometer range displacements at varying sinusoidal amplitudes on the specimens. A multi-contact electrode array (MEA) with 50um gold Pt contacts was attached on the bottom of a Petri dish that was filled with normal saline and a 200µm thick PVDF-TrFE specimen was placed on top of the array. The surface area of the array and the piezo specimen was about 1x2mm. The specimen was sandwiched between the MEA and a horizontal Plexiglas piece that was mechanically moved in the vertical direction in small peak-to-peak amplitudes adjusted from 10-110µm at 3 Hz frequency. The voltage induced was recorded through a 100-gain low-noise amplifier and collected into the computer through a data acquisition board at 1000 samples per second. The peak-to-peak amplitude of the sinusoidal signals induced on the MEA contacts were analyzed in Matlab and plotted as a function of displacement amplitudes in Figure 5. The figure shows the peak-to-peak piezo electric voltage after being divided by the gain of the amplifier. The slope of a linear line fit is about 2.33 µV/µm. The intercept is at around 40µm suggesting that a minimum displacement is needed to start generating piezo voltages.

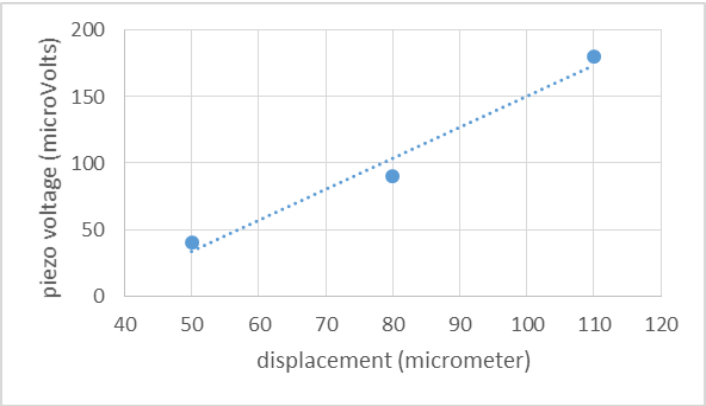

Figure 5. Voltage output from PVDF-TrFE scaffolds as a function of displacement.

The experimental setup was optimized in order to deform the PVDF-TrFE material using small yet measureable displacements and measure resulting electrical output. A commercially available piezoelectric (PZT) material from PiezoSystem Inc. was used to produce micron level perturbations on our PDVF-TrFE mesh. The PZT was about a 2.5cm long beam and it could bend under large voltage. The tip of the beam moved down about 50um when 200V was applied and the displacement changed linearly between 110-200V (Figure 6). A long glass tube (1mm. diam) was attached to the tip of the beam vertically and transferred the displacement to the materials under testing while providing electrical isolation. This separation between the PZT beam and the material under testing eliminated the electrical artifacts in the recorded signals from the tested material. The testing material was sandwiched between a plate attached at the end of the glass tube and the solid floor in a Petri dish, which was filled with diluted PBS in order to reduce conductivity and mimic the actual impedances seen in the neural tissue as reported earlier by others and confirmed by our impedance measurements of electrode implants in our lab. The PVDF-TrFE mesh pad had a thickness of ~180um and it was cut into a 2x2mm sheet. A multi-electrode array (4x8 contact) with 50um diam. contacts were placed under the piezoelectric material to measure the electrical field generated by the material. Small contact size ensured the electrical fields were not averaged out spatially by highly conductive electrode contacts. Having a large number of contacts allowed us to sample the electrical field at multiple points and thus increase the confidence level in the measurements. The multi-channel voltages from the array were amplified by a gain of 800 and collected into the computer through a National Instruments data acquisition board and Matlab software at a sampling frequency of 10,000 Hz, a high rate to capture fast transitions in the voltage.

A square wave with 100ms ON and 400ms OFF cycles were applied to the PZT beam to produce displacements in the 0-50um range. During the ON cycle, the beam goes down instantly and applies the full displacement on the specimen, which coincides with a sharp increase in the electrical filed in the recorded signals. The voltage declines slowly after the initial increase, as a reflection of the fact that no voltage is produced by the material under steady conditions without displacement (Figure 7). The peak voltages were measured from all contacts and averaged (after removing the outliers) from multiple perturbation trials and plotted against the displacement in Figure 8. The voltage peaks increase almost linearly with increasing displacement. The control specimen (PCL) did not produce any voltages using this setup where electrical and mechanical artifacts were eliminated. With this characterization data in hand, now we can much better evaluate the electrical field measurements from electrodes implanted in animals.

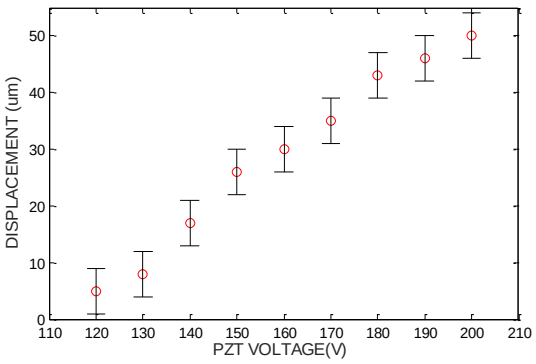

Figure 6. Displacement exerted on the specimen as a function of driving voltage applied to the PZT beam.

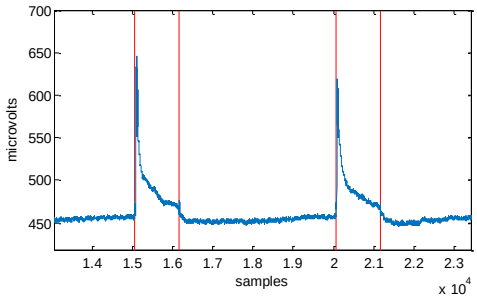

Figure 7. Raw signal of PVDF-TrFE recorded through one of the contacts in the multi-electrode array. The mechanical displacements are applied between the red lines.

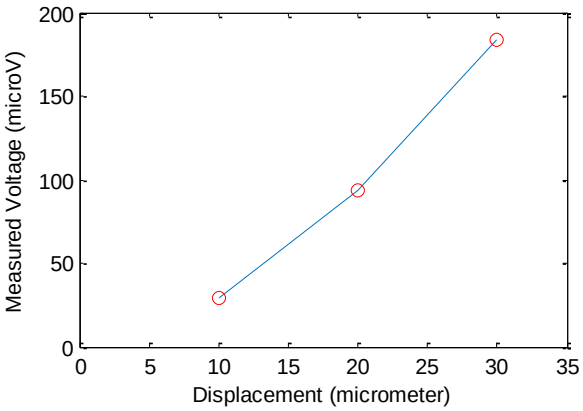

Figure 8. Average of the voltage peaks measured from PDVF-TrFE using an array electrode as a function of displacement.

We were able to generate unprecedented data by measuring electrical output in conditions that mimic the wet environment in live tissue. The unforeseen details about the experimental setup to remove the electrical and mechanical artifacts from the electrical recordings took additional time and delayed our transition to animal implantation. We will begin implanting electrodes coated with PVDF-TrFE meshes in year 2 with the preparation of a publication for submission based on the data collected from the *in vitro* experiments. Dr. Sahin's lab has extensive experience implanting similar electrodes into the rat spinal cord and thus we foresee a quick transition into the next set of experiments.

3.2. ***In vitro*** **studies of SC growth and SC co-cultures with dorsal root ganglion (DRG) to evaluate neurite extension on piezoelectric scaffolds**

In Vitro **Studies of Schwann Cell Survival and Viability on Piezoelectric Scaffolds.** Rat SCs, isolated from adult sciatic nerve and transfected to express GFP, provided by the Bunge Lab, were cultured on aligned PVDF-TrFE fibers for up to 7 days using standard growth media for SCs. Experimental groups were aligned PVDF-TrFE fibers coated with or without Matrigel (BD Biosciences) to correspond to *in vivo* studies. Laminin coated tissue culture polystyrene were used as a control for all the studies. SC survival was assessed by changes in cell number and ATP activity using the ATP assay (CellTiter-Glo Luminescent Cell Viability Assay, Promega, Madison WI, US) over time at 1, 4, and 7 days. Cell morphology and attachment was assessed by using confocal microscopy. As shown in Figure 9, cells attached to both coated and uncoated aligned fibers where cells elongated along the length of the fiber. Cell numbers appeared less on uncoated fibers and this was verified quantitatively using the ATP assay (Figure 10). The results show that the matrigel coated fibers had significantly higher ATP and cell numbers over time than on uncoated fibers ($p<0.05$).

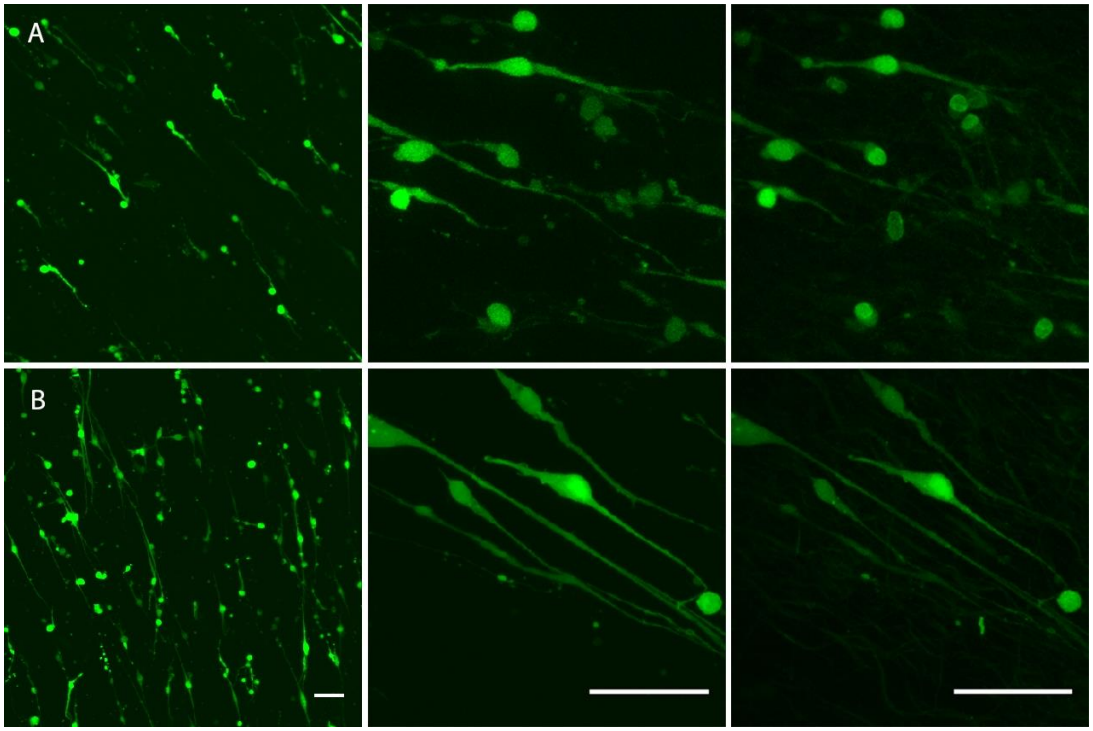

Figure 9. Confocal microscope images of GFP-SCs on PVDF-TrFE aligned (A), Matrigel-coated aligned (B) fibrous scaffolds at day 7 (left to right: 20X, 60X, and 60X showing fibers (autofluorescence) of the scaffold, scale bar = 50 μm).

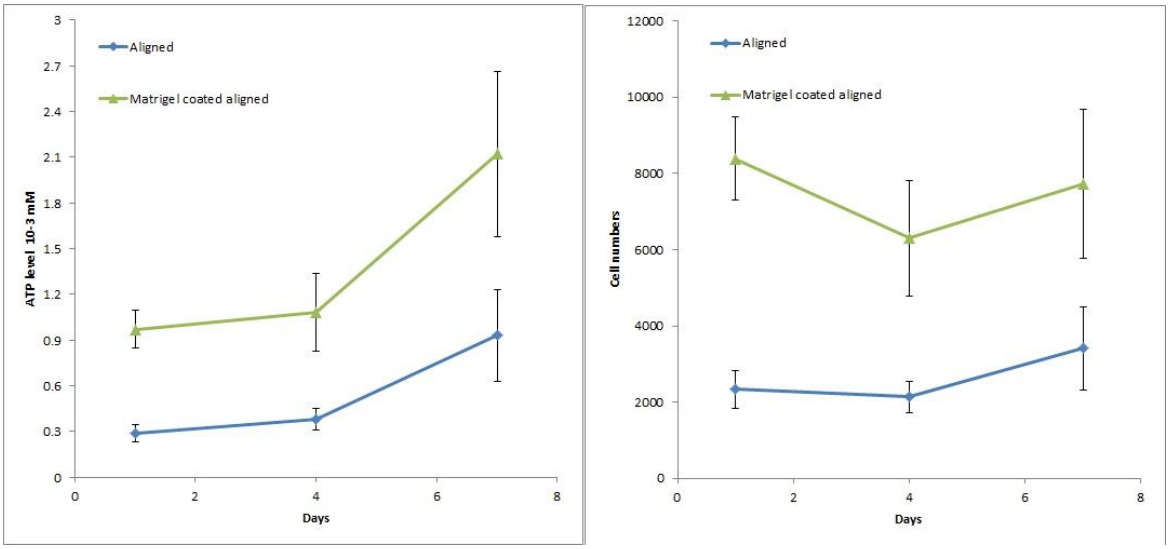

*Figure 10. ATP levels (left) and cell numbers (right) for SCs cultured on PVDF-TrFE fibrous scaffolds. ATP levels for SCs on Matrigel-coated scaffolds were significantly higher than uncoated scaffolds at days 1, 4 and 7 (*p<0.05). ATP levels for SCs at day 7 were significantly higher than at days 1 and 4 for uncoated and Matrigel-coated scaffolds (#p<0.05). Cell numbers for SCs on Matrigel-coated scaffolds were significantly higher than on uncoated scaffolds at days 1, 4 and 7 (*p<0.05).*

We also determined the optimum seeding density for SC growth on the fibrous scaffolds prior to performing neurite extension studies. We seeded 3,000, 6,000, and 15,000 SCs on 6

mm diameter PVDF-TrFE fibrous disks. 15,000 cells was the original seeding number used in all prior experiments. 3,000 cells did not increase in cell number over time (data not shown). 6,000 and 15,000 cells continued to grow over time (Figure 11). Cell morphology and attachment was assessed by using confocal microscopy. As shown in figure 12, SCs attached well for both seeding densities.

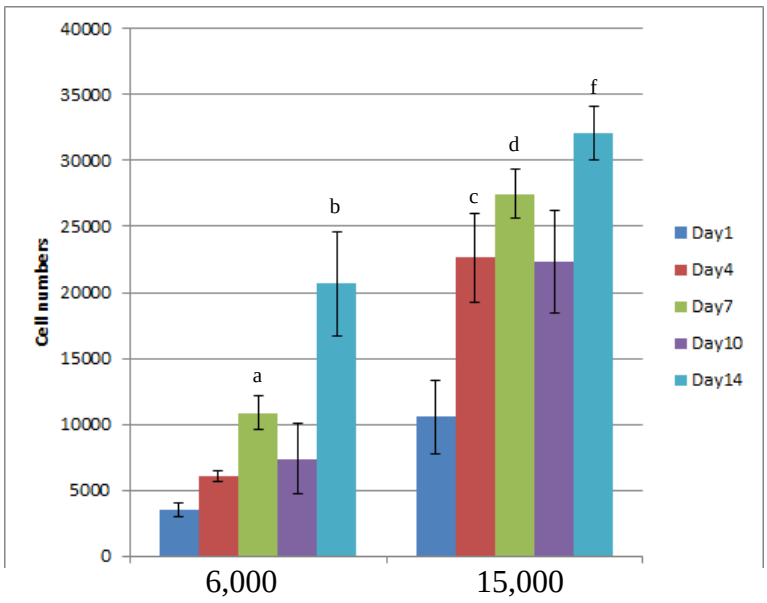

Figure 11: SCs grown on PVDF-TrFE aligned fiber scaffolds for up to 14 days. Different seeding densities were investigated. [a]p<0.05, day 7 is significantly higher than days 4 and 1. [b]p<0.05, day 14 is significantly higher than all other time points. [c]day 4 is significantly higher than day 1. [d]day 7 is significantly higher than day 1, [e]day 10 is significantly higher than day 1, and [f]day 14 is significant higher than days 1, 4 and 10.

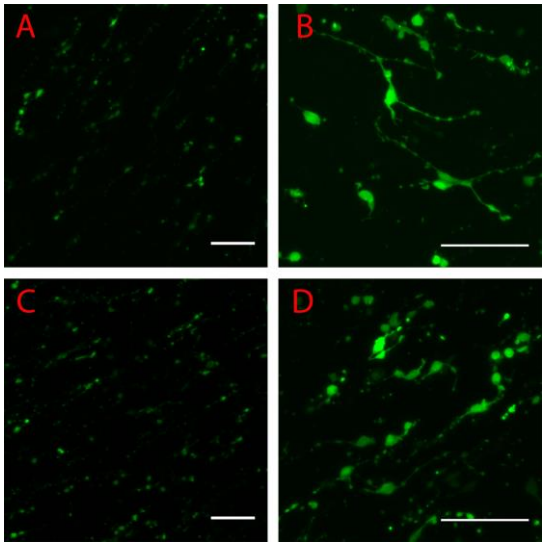

Figure 12. Confocal microscope images of GFP-SCs seeded at a&b) 6,000 and c&d) 15,000 cells on PVDF-TrFE aligned scaffolds at day 7 (a&c - 20X, b&d – 60X, scale bar = 100 μm).

We also investigated SCs transduced with a bifunctional neurotrophin (D15A) to establish their growth on the PVDF-TrFE fibers since they will be used in Aim 2/Year 2 for neurotrophin release. Experimental groups were aligned PVDF-TrFE fibers having nano or micron-sized fiber diameters and coated with or without Matrigel to correspond to *in vivo* studies. All PVDF-TrFE scaffolds were annealed. Laminin coated and Matrigel coated tissue culture polystyrene were used as a control for all the studies. SC growth was assessed by changes in cell number by the pico green assay (DNA measurement) (Invitrogen, Inc.) over time at 1, 4, and 7 days. Cell morphology and attachment was assessed by using confocal microscopy. As shown in Figure 13, both D15A-SCs (GFP D15A) and unmodified SCs (GFP) attached to both coated and uncoated aligned fibers for both nano and micron-sized fiber dimensions. As expected, cell numbers appeared less on uncoated fibers and this was verified quantitatively using the pico green assay (Figure 14). The results show that the matrigel coated fibers had significantly higher cell numbers over time than on uncoated fibers ($p<0.05$).

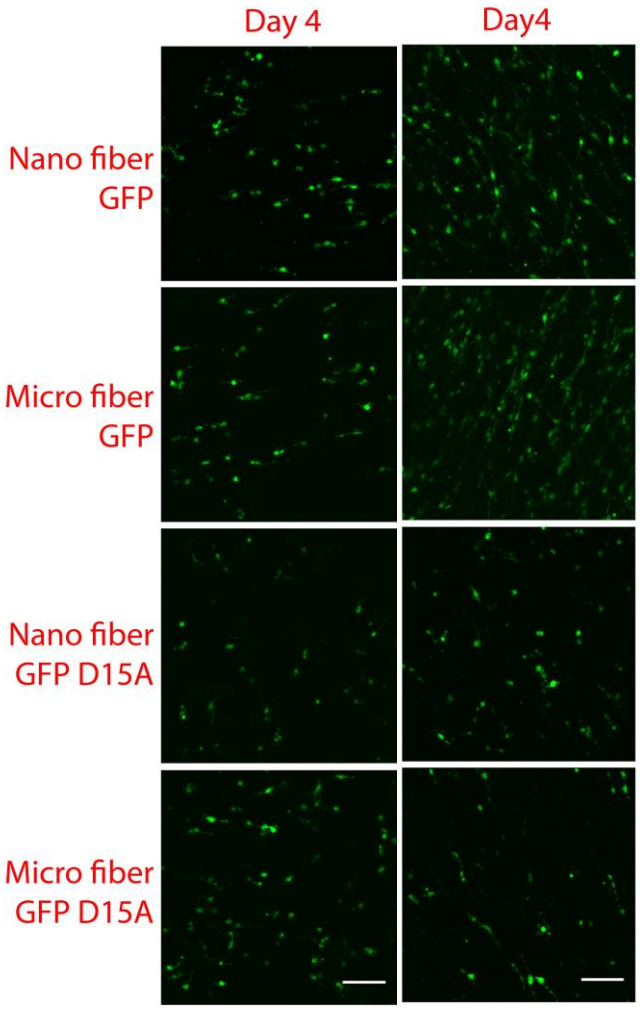

Figure 13. Confocal microscope images of GFP-SCs (GFP) and D15A-GFP-SCs (GFP D15A) on PVDF-TrFE aligned scaffolds either uncoated or coated with Matrigel at day 4 (20X, scale bar = 50 μm).

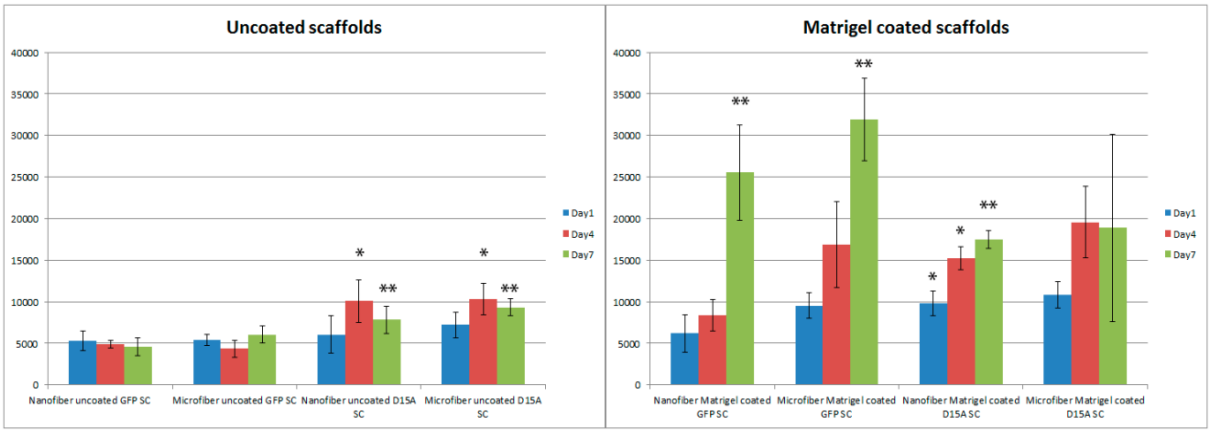

*Figure 14: Cell numbers for GFP-SCs and D15A-SCs cultured on PVDF-TrFE scaffolds uncoated (left) and coated with Matrigel (right). (Left) *GFP D15A SCs seeded on uncoated fibers (both nano and micro fibers) were significantly higher in cell number at Day 4 compared to GFP SCs at Day 4 ($p<0.05$). (Left) **GFP D15A SCs seeded on uncoated fibers (both nano and micro fibers) are significantly higher in cell numbers at Day 7 compared to GFP SCs at Day 7. No significant difference in cell number was observed from day 1 to day 7 for all uncoated scaffolds groups for both GFP D15A SCs and GFP SCs. SC cell numbers were maintained during culture. No significant difference was observed between nano fibers and micro fibers. (Right) *GFP D15A SCs seeded on Matrigel coated nano fibers were significantly higher in cell number at days 1 and 4 compared to GFP SCs at days 1 and 4. (Right) ** Cell numbers were significantly higher at day 7 as compared to days 1 and 4. No significant difference was observed between nano fibers and micro fibers.*

In addition, no differences in cell numbers were detected between micron-sized and nano-sized fibers, which was important to establish for the conduit design for the *in vivo* studies. Micron-sized fibers were used inside of the conduit for *in vivo* studies because they have larger interfiber spacing than nano-sized fibers which is important for SC infiltration throughout the fibrous construct. D15A-SCs had a higher proliferation rate than unmodified cells. As shown in these studies, the D15A cells had higher numbers than unmodified SCs on uncoated as well as coated fibers. D15A-SCs also had a higher proliferation rate than SCs on tissue culture polystyrene controls up through day 7. By day 7, D15A-SCs on Matrigel coated scaffold achieved confluence and began to detach from the scaffolds, as indicated by the lower cell numbers at this time point as compared to SCs (Figure 14 – Right). Studies using lower cell seeding densities may be more favorable for neurotrophin release studies in Aim 2/Year 2.

SC Co-Culture with DRG and Measurement of Neurite Extension

GFP SCs were seeded at different densities onto PVDF-TrFE aligned fibers coated with or without Matrigel and cultured for 4 days D10 media. At day 4, DRGs isolated from E17 rat embryos were seeded on the SC-laden scaffolds and the co-culture was maintained for 2 days in D10 media or D10 containing nerve growth factor (NGF) media. D10 is the standard growth media for SCs and D10 with NGF is used to support DRG growth. The coculture was fixed using 4% paraformaldehyde and stained for neurofilament. Neurite extension was assessed by measuring 10 longest axons for each DRG. DRGs extended neurites on both uncoated and coated fibers and with or without SCs (Figure 15) however, the greatest neurite extension occurred for 6,000 and 15,000 SC seeding density on matrigel coated scaffolds in

D10+NGF media (Table 2). Findings from these studies establish the co-culture conditions for the neurotrophin release studies that will occur in Aim 2/year 2 of this project. 6000 SC seeding density, Matrigel coating and the use of D10+NGF media will be used in year 2 studies. Detecting myelination was originally proposed in these cultures however for myelination to occur, cultures have to be maintained for several weeks. The culture surface was not large enough to conduct the DRG-SC culture for an extended period because of the significant neurite extension. The culture surface area will need to be increased to perform extended culture periods to detect myelination, which can be performed in year 2 with the neurotrophin release studies.

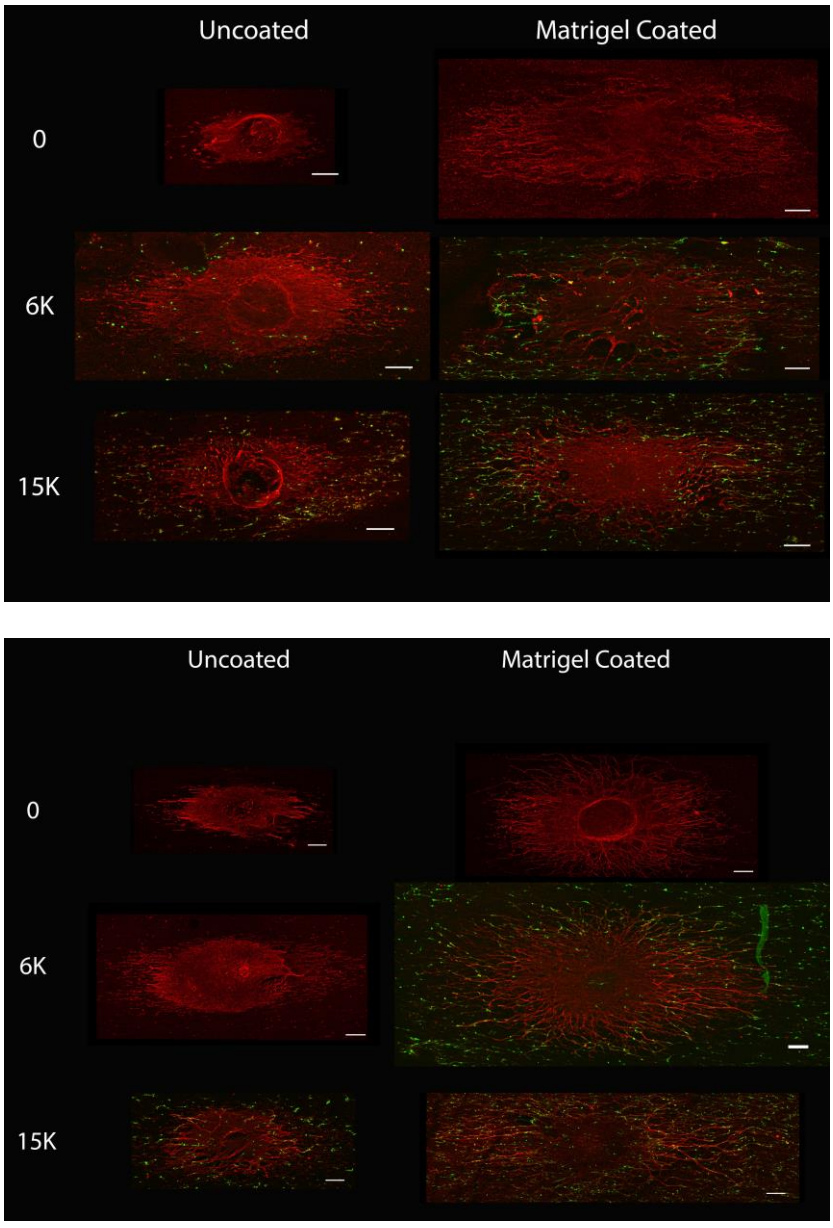

Figure 15: GFP labeled SCs seeded at different seeding densities in co-culture with DRGs on PVDF-TrFE fibers either uncoated or coated with Matrigel at X days. SCs are green and DRG are stained for neurofiliament (Red). Top panel shows neurite extension for D10 media (standard growth media for SCs) and Bottom panel shows neurite extension for D10 with NGF added to the media (media for growth of DRG). Scale bar is 200 μm.

Table 2: Neurite extension on aligned piezoelectric fibers seeded with varying densities of SCs in D10 or D10 with NGF containing media. (Values are Mean+/-S.D. Units are μm).

D10 Media

	Uncoated	Matrigel coated
0 SCs	240.14 ± 83.02	927.82 ± 202.16[a]
6K SCs	610.07 ± 179.38[d]	1064.39 ± 150.81[a]
15K SCs	685.48 ± 180.60 [d]	991.91 ± 174.55

D10+NGF Media

	Uncoated	Matrigel coated
0 SCs	368.87 ± 189.89	1056.00 ± 140.50[e]
6K SCs	1042.41 ± 182.14[d]	1560.27 ± 235.96[b,c]
15K SCs	605.89 ± 109.35	1467.27 ± 178.08[b,c,e]

[a]$p<0.05$, Matrigel coated groups are statistically higher than uncoated groups at the same seeding density in D10 media. [b]$p<0.05$ for Matrigel coated groups at 6K and 15K seeding density in comparison to 0 SCs. [c]$p<0.5$, significantly greater for all groups in D10 media. [d]$p<0.05$, significantly greater than 0 SCs for the uncoated groups. [e]$p<0.05$, statistically greater than uncoated group in D10+NGF media at the same seeding density.

3.3. *In Vivo* Studies of the Piezoelectric Conduit using the Complete Transection Model in the Rat

The complete transection model studies were performed in Dr. Bunge's laboratory at the University of Miami.

Study 1: Fiber filled vs hollow conduits. A 3-week study was performed to compare the effect of (1) fiber filled conduits (conduits filled with aligned fibers consisting of 4 aligned fibrous layers) and pre-loaded with GFP SCs without Matrigel and (2) hollow conduits containing Matrigel and GFP SCs at the time of transplantation on axonal growth. The goal of this study was to evaluate whether fiber filled conduits enhanced axonal growth without the use of Matrigel. Comparisons were made with our established protocol of using SCs suspended in Matrigel and injected into the hollow conduits. Surgical methods are described below. Animals were euthanized 3 weeks post transplantation and cryocut into 20μm thick sagittal sections. Immunostaining of SC bridges in hollow (Figure 16A) and fiber filled (Figure 16B) conduits was performed for transplanted SCs (green fluorescent protein, GFP), astrocytes (glial fibrillary acidic protein, GFAP), and axons (heavy chain neurofilament, RT97). Although more SCs were observed in the hollow (Figure 16A&C) compared to the fiber filled (Figure 16B&D) conduits, more axons were observed to grow into the conduit and toward the caudal SC/host interface using the fiber filled conduits (Figure 16C and D), suggesting the fibrous layers provided contact guidance for axons to grow. Close association of $RT97^+$ axons with SCs was observed in both hollow (Figure 16C) and fiber filled (Figure 16D) conduits. DBH^+ brainstem axons grew beyond the rostral host-SC interface and onto the fibrous layers of the fiber filled (Figure 16F) conduits in the rostral to caudal direction. In the hollow (Figure 16E) conduits, DBH^+ brainstem axons were positioned randomly and only at the rostral host-SC interface. $CGRP^+$ (Calcitonin gene-related peptide) sensory axons were observed at the caudal host-SC interface in hollow (Figure 16G) conduits. $CGRP^+$ sensory axons were closely associated with SCs along the caudal to rostral direction on the fibrous layers in the fiber filled (Figure 16H) conduits. BBB and incline plane tests were done weekly post transplantation. At 3 weeks, no statistical differences were observed between groups in BBB or incline plane scores (Figure 17).

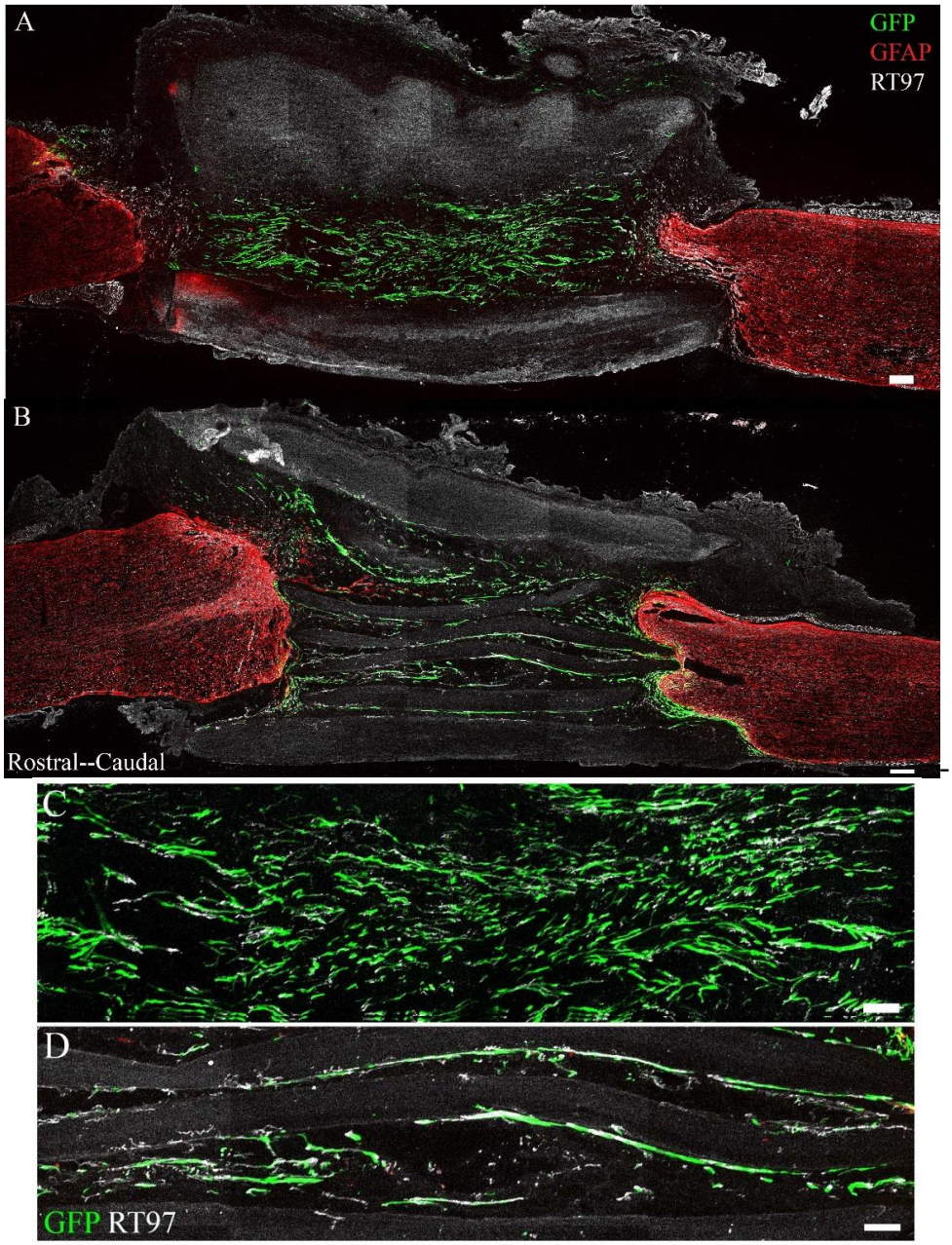
A
GFP
GFAP
RT97
B
Rostral--Caudal
C
D
GFP RT97

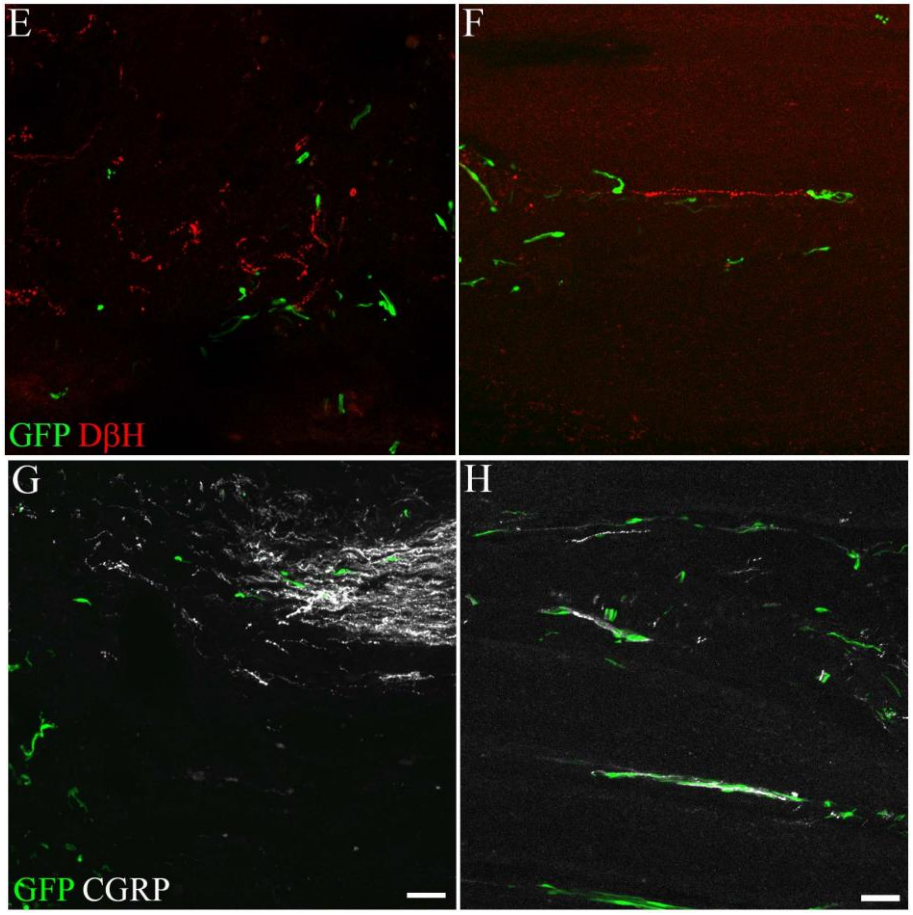

Figure 16. Confocal fluorescent images of: SC hollow (A) and fiber filled (B) conduits 3 weeks post-transplantation for (scale bar = 200µm); RT97^{+} axons (general axon marker) were closely associated with transplanted GFP SCs in the middle of the transplant in hollow (C) and fiber filled (D) conduits (scale bar = 100 µm); DBH^{+} axon (dopamine beta-hydroxylase, brainstem axons) staining at the rostral host/SC interface in hollow (E) conduits and in between the layers at the rostral end of the fiber filled (F) conduits. CGRP^{+} axons (Calcitonin gene-related peptide, sensory axons) at the caudal host/SC interface in hollow (G) conduits and in between the layers at the caudal end of the fiber filled (H) conduits.

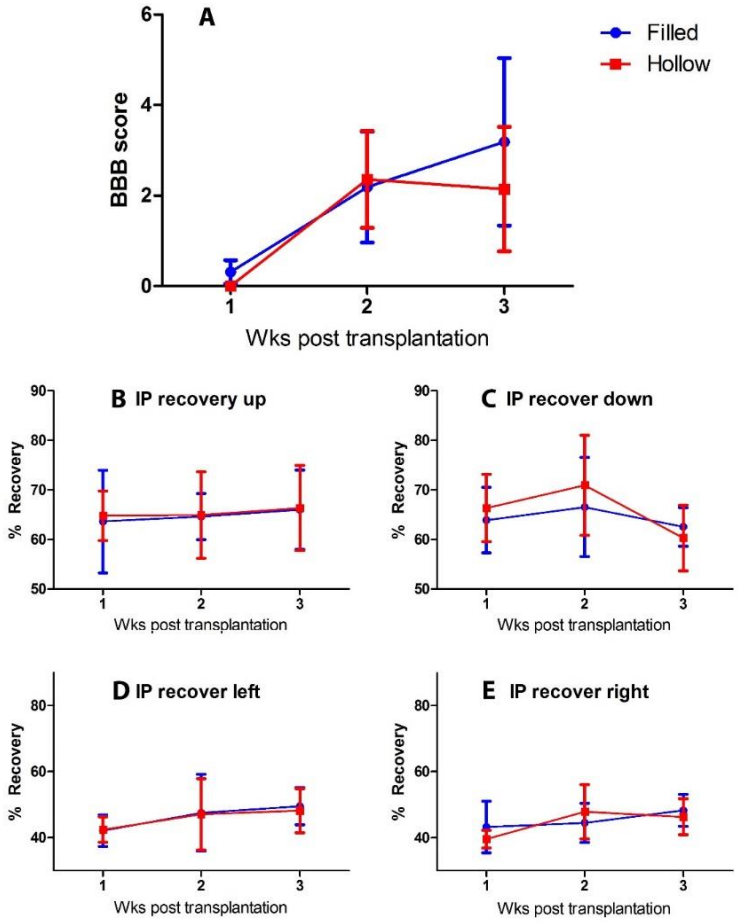

Figure 17: Weekly BBB score (A) and incline plane (IP) recovery at 4 positions (B-E) post transplantation of fiber filled (filled) (blue) or hollow (red) conduits. No statistically significant differences detected for BBB scores and IP recovery.

Study 2: Evaluating the influence of Matrigel in fiber filled conduits. A 6-week study was performed to investigate improvement in SC survival by (1) coating the fiber filled conduits with Matrigel prior to transplantation or (2) injecting Matrigel with SCs at the time of transplantation within the fiber filled conduits and its effect on directional axon growth in the fiber filled conduits. The experimental groups were as follows:

- Group **MM**: Matrigel coated and pre-loaded with GFP SCs in the fiber filled conduit + injection of GFP SCs with Matrigel/DMEM/F12 between the fibrous layers at the time of transplantation.
- Group **MD**: Matrigel coated and pre-loaded with GFP SCs in the fiber filled conduit + injection of GFP SCs with DMEM/F12 only between the fibrous layers at the time of transplantation.
- Group **DM**: Pre-loaded with GFP SCs in the fiber filled conduit + injection of GFP SCs with Matrigel/DMEM/F12 between the fibrous layers at the time of transplantation.
- Group **DD**: Pre-loaded with GFP SCs in the fiber filled conduit + injection of GFP SCs with DMEM/F12 only between the fibrous layers at the time of transplantation.

In groups MM and MD, fiber filled conduits were coated with Matrigel by placing them in a matrigel solution overnight and rinsed with PBS prior to pre-loading with GFP-SCs. GFP-SCs were pre-loaded into the fiber filled conduits in all groups described in later sections. At the time of transplantation, a mixture of GFP-SCs/DMEM-F12/Matrigel was injected between the fibrous layers in groups MM and DM. In groups MD and DD, only a mixture of GFP-SCs/DMEM-F12 was injected.

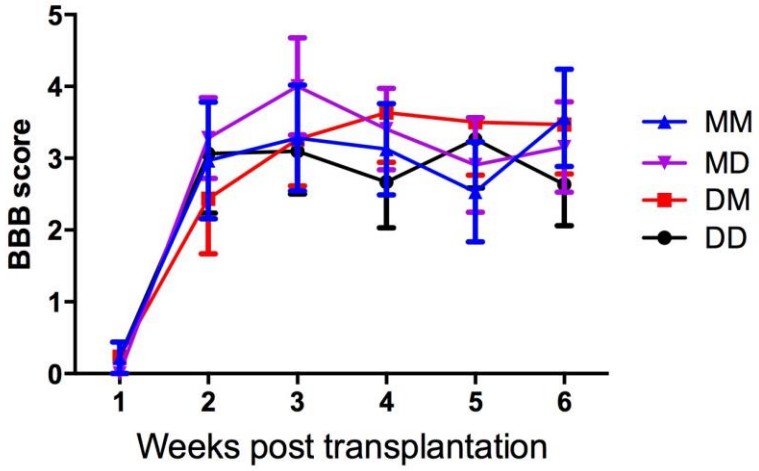

Figure 18. Weekly BBB scores post transplantation for groups MM, MD, DM, and DD.

No significant differences were observed in weekly BBB scores among the groups (Figure 18). Animals were euthanized 6 weeks post transplantation and cryocut into 20µm thick sagittal sections. Immunostaining of SC conduits in groups MM, MD, DM, and DD was performed for transplanted SCs (GFP), astrocytes (glial fibrillary acidic protein, GFAP), and axons (heavy chain neurofilament RT97) in Figure 19. SC survival was observed in all the groups. Axon regeneration into the SC conduits appeared to be more for the groups MM and DM where Matrigel was injected with SCs at the time of transplantation. Group DD, the only group without Matrigel, exhibited the least GFP SCs and axons compared to the other groups.

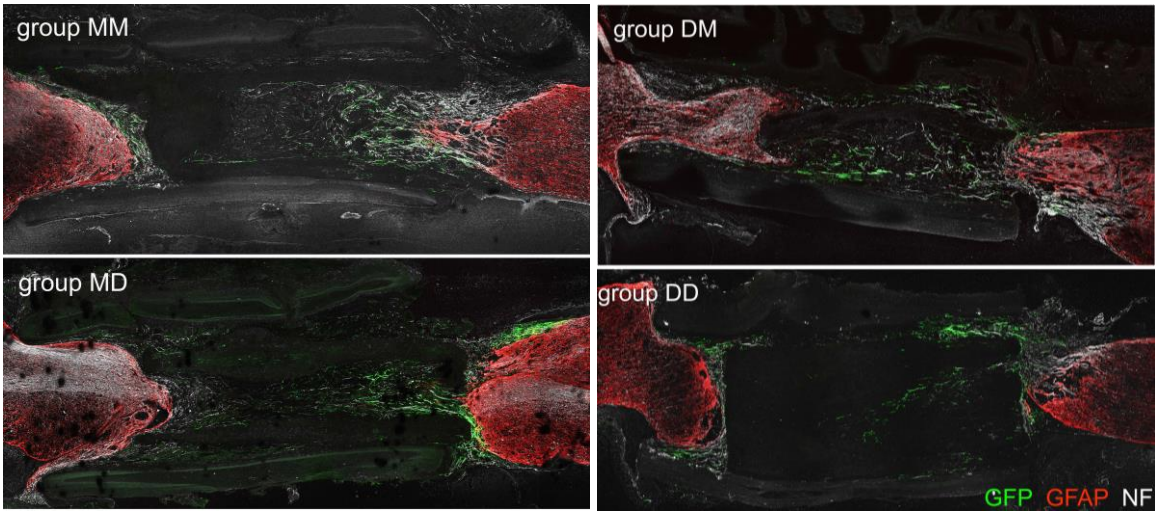

Figure 19. Confocal immunofluorescent images of transplanted GFP SCs (green), astrocytes (GFAP, red) and axons (NF, white) in SC bridges (left is rostral) 6 weeks post-transplantation of groups MM, MD, DM, and DD. The layers within the conduits can be observed in Figure 1.2.5.

1μm transverse plastic sections of groups MM, MD, DM, and DD are shown in Figure 20. Abundant blood vessels were observed in all groups in between the fibrous layers within the conduit. Both unmyelinated and myelinated axons were observed in groups MM and DD with transmission electron microscopy (TEM) (Figure 21). Clusters of unmyelinated and myelinated axons were observed in group DD but were more evenly distributed throughout the transplant in group MM.

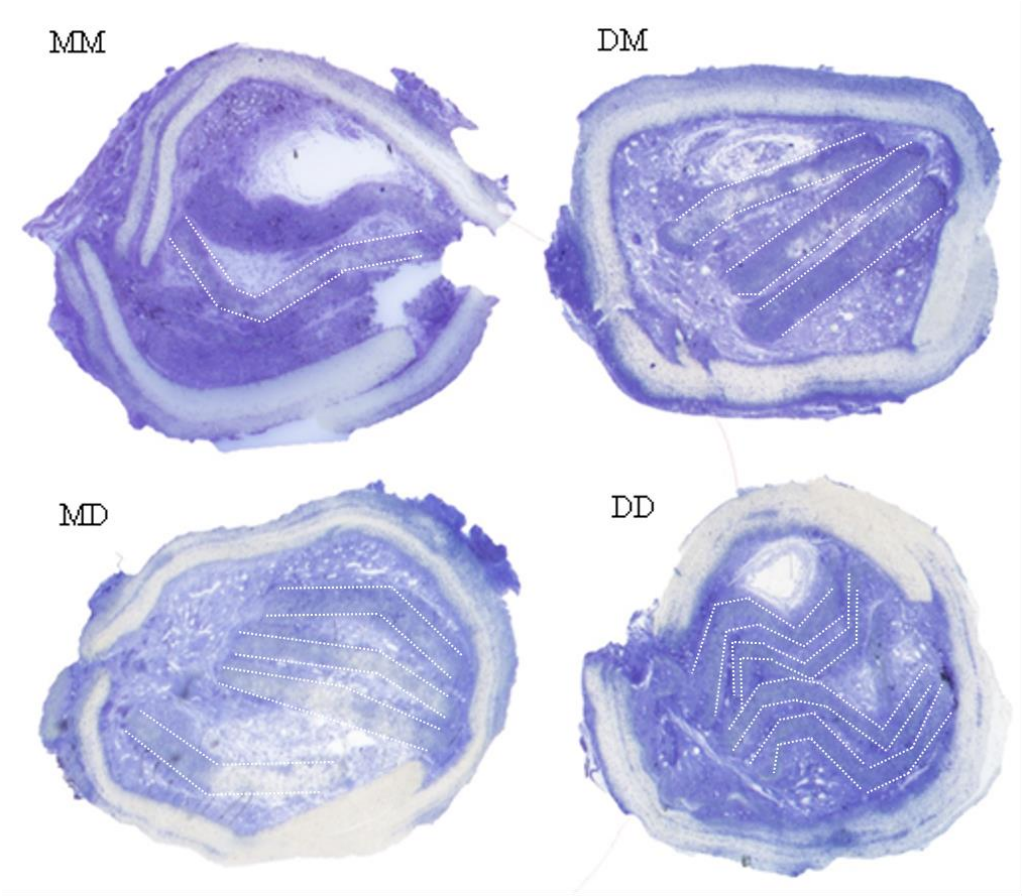

Figure 20. Bright field images of 1μm transverse plastic sections stained with toluidine blue of groups MM, MD, DM and DD. Layers are outlined in white dashed lines in the conduits.

Figure 21. Transmission electron microscopy (TEM) images for groups MM and DD (Mag = 10500x).

We are completing the quantitative analyses for 1) myelinated and unmyelinated axons using TEM, 2) myelinated axons and blood vessels using the transverse plastic sections, and 3) ascending ($CGRP^+$, calcitonin gene-related peptide) and descending ($D\beta H^+$, dopamine beta-hydroxylase and $5HT^+$, serotonin) axons and $GFAP^+$ processes using the sagittal sections. We are also identifying fibroblast , endogenous SCs, and immune cells by immunostaining with fibronectin, P75, and Iba1, respectively. The quantitative results will compliment our observations that the Matrigel injected conduits were more favorable for SC survival and axonal growth. Matrigel injection into the fiber filled conduits will be used in Aim 2/year 2 studies examining neurotropin release.

Methods

GFP-SC loading into fiber filled conduits. The loading method of GFP-SCs into fiber filled conduits prior to implantation between the transected stumps of rat spinal cords was developed. A GFP-SC suspension and a fiber filled conduit were placed in a syringe with a three-way stopcock attached. All valves of the three-way stopcock were closed and GFP-SCs were vacuum loaded into the fiber filled conduits and then incubated at 37C for two hours. GFP-SCs were observed on the interior wall of the conduit (Fig 22A) and within all layers in the conduit. GFP-SCs showed similar attachment in all layers and one layer is shown in Fig 22.

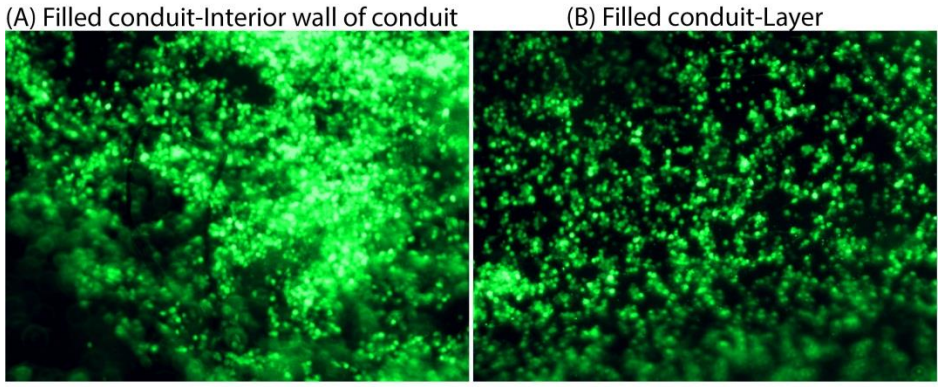

Figure 22. Confocal images of GFP-SCs vacuum loaded into fiber filled conduits and incubated for 2 hours prior to implantation. A) GFP-SCs on the interior wall of the conduit and B) GFP-SCs on one of the fibrous layer inside the conduit.

Surgical Technique. An outline of the surgical procedure is as follows (Figure 23): T7-T9 vertebrae were exposed in adult Fischer rats (A) and laminectomy was performed from T7-T9 (B). The spinal cord was completely transected at T8 creating a 2-3mm gap between the rostral and caudal stumps (C). For animals receiving a hollow conduit and SC/Matrigel injection: A hollow conduit was inserted between the rostral and caudal stumps with two pre-cut windows on the dorsal surface (D). The GFP-SC and Matrigel mixture was then injected into the hollow conduit via one of the pre-cut windows and both windows were closed after injection (E). For animals receiving fiber filled conduits: A fiber filled conduit already pre-loaded with GFP-SCs was inserted between the rostral and caudal stumps (F). For animals receiving a fiber filled conduit plus injection of SC/Matrigel: a fiber filled conduit with two pre-cut windows was inserted between the rostral and caudal stumps with the windows on the dorsal surface. The SC/Matrigel mixture was then injected between the layers via one of the pre-cut windows and then both windows were closed after injection.

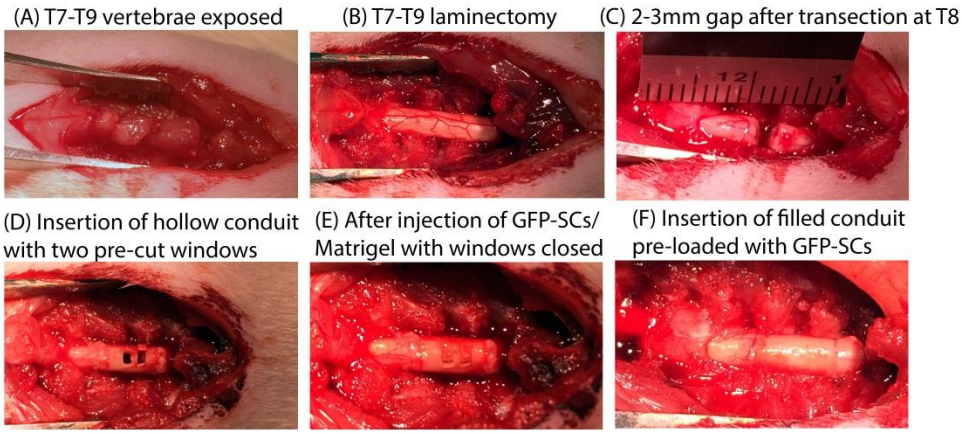

Figure 23: Images of the surgical implantation procedure for conduits, either filled with Matrigel and GFP-SCs or pre-loaded with GFP-SCs in fiber filled conduits, in the rat complete transection model.

Quantification method for immunofluorescent sections. Number of $GFAP^+$ processes can be used as an indicator for permissive interface between the host cord and transplant. $GFAP^+$ processes were also closely associated with axon regeneration into the transplant where more processes suggested a more permissive interface. The goal is to quantify $GFAP^+$ processes and ascending ($CGRP^+$, calcitonin gene-related peptide) and descending ($D\beta H^+$, dopamine beta-hydroxylase and $5HT^+$, serotonin) axons across the SC conduit in 20μm sagittal sections with the following protocol (Figure 24):

i. Definition of R0 and C0
    i. The most distal point in the rostral cord (R0) and the most proximal point in the caudal cord (C0) of the bulk presence of astrocytic cell bodies.
ii. Definition of the following distances from R0 and C0
    i. Definition of 0.25, 0.5, 1, 1.5 and 2mm caudal from R0 and denoted as R0.25, R0.5, R1, R1.5, and R2, respectively.
    ii. Definition of 0.25, 0.5, 1 and 1.5mm rostral from C0 and denoted as C0.25, C0.5, C1, and C1.5, respectively.
    iii. Definition of 0.5 and 1 mm caudal from C0 and denoted as C-0.5 and C-1, respectively. This should only contain caudal spinal cord only.
iii. At each distance along the conduit (except at C-0.5 and C-1), draw a dorsal-ventral line and measure the length of:
    i. Exterior walls of conduit (E1 and E2),
    ii. Inner layers within the conduit (L1 to L4),
    iii. And inter-layer spaces (M1 to M5).
    iv. Count the number of descending and ascending axons and $GFAP^+$ processes that cross each dorsal-ventral line at each distance.
iv. At C-0.5 and C-1, draw a dorsal-ventral line defining the width of the caudal cord. Count the number of descending and ascending axons that cross each dorsal-ventral line.

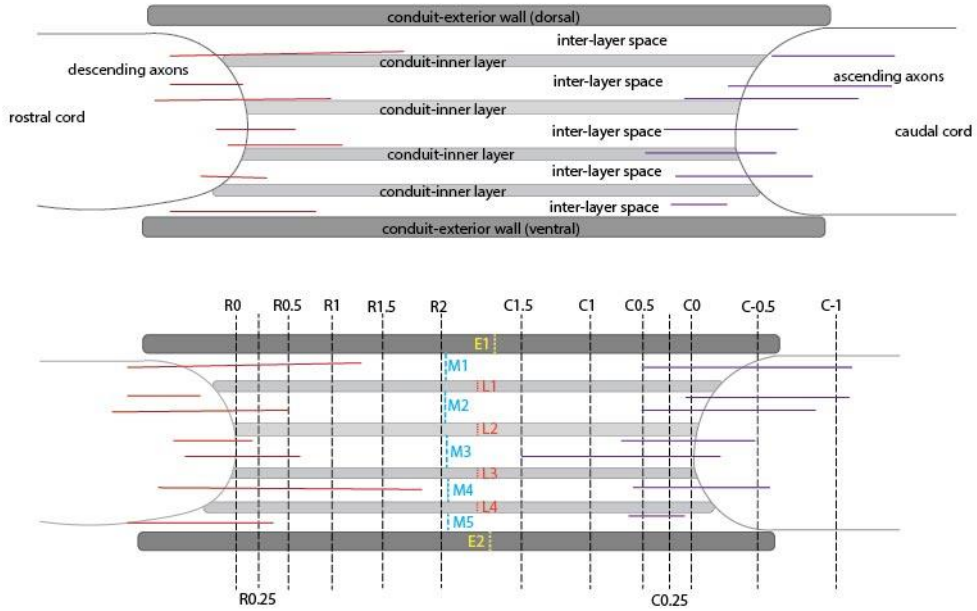

Figure 24. Parameters for quantifying the number of GFAP$^+$ processes and ascending (CGRP$^+$, calcitonin gene-related peptide) and descending (DβH$^+$, dopamine beta-hydroxylase and 5HT$^+$, serotonin) axons across the SC conduit in 20μm sagittal sections. The conduit is composed of an exterior wall (dark grey area), inner layers (lighter grey area), and the spaces between layers and the exterior wall, defined as inter-layer spaces (white areas). Numbers of descending axons (red) and ascending axons (purple) and GFAP$^+$ processes (not denoted) crossing each dorsal-ventral line at each distance from R0 and C0 are counted. The dorsal-ventral line at each distance is composed of width of exterior wall (E1 and E2), inner layers (L1 to L4), and inter-layer spaces (M1 to M5).

Quantification method for plastic sections. The goal is to quantify myelinated axons and blood vessels in 1μm transverse plastic sections with the following protocol (Figure 25):

i. Take an image of the section at 60x.
ii. Count the number of myelinated axons and blood vessels in each defined area.

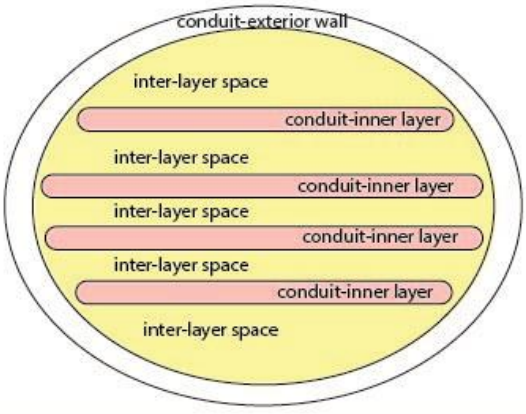

Figure 25. Parameters for quantifying the number of myelinated axons and blood vessels in 1μm transverse plastic sections. The conduit can be divided into three areas: exterior wall (white), layers within the conduit (pink) and inter-layer spaces (yellow).

What opportunities for training and professional development has the project provided?
Individual mentoring was provided to two PhD students, Siliang Wu and Sinan Gok, at New Jersey Institute of Technology. Individual mentoring also was provided to one postdoctoral fellow, Yee-Shuan Lee, at the University of Miami.

How were the results disseminated to communities of interest?
In the summer, the PI is an active mentor in K-12 programs that showcase this research. FEMME 8 program, which introduces approximately 30 underrepresented minority, female 8th graders to science and engineering, tour the PI's laboratory and are involved in hands-on experiments related to this project. The PI also gave a presentation in the CHIME program which introduces approximately 20 underrepresented minority junior high and high school students to science and engineering on July 15, 2015.

What do you plan to do during the next reporting period to accomplish the goals?
We will perform the year 2 objectives as described in the major activities. We will determine if axons extend into the caudal spinal parenchyma following the controlled release of neurotrophins at and below the SC conduit and improve functional recovery.

1. *In vitro* characterization of the controlled release of NT3 and BDNF from the fibrous piezoelectric scaffolds will be evaluated for neurite extension and SC survival, Period: 13-24 months
2. *In vitro* characterization of the controlled release of NT3 and BDNF from the PEO hydrogel will be evaluated and DRG neurite outgrowth measured, Period: 13-24 months.
3. A pilot in vivo study will be performed to determine axon growth into, through and out of the SC- piezoelectric conduit with NT3 and BDNF release, Period: 19-24 months.

4. IMPACT
What was the impact on the development of the principal disciplines of the project?
The impact of this work will be in the fields of neuroscience, regenerative medicine and biomaterials. The findings will demonstrate this combination therapy using novel electroactive fibrous conduits can affect axonal guidance and regeneration.

What was the impact on other discipline?
Nothing to Report.

What was the impact on technology transfer?
Nothing to Report.

What was the impact on society beyond science and technology?
Nothing to Report.

5. CHANGE/PROBLEMS
Changes in approach and reasons for change
Nothing to Report.

Actual or anticipated problems or delays and actions or plans to resolve them

Nothing to Report.

Changes that had a significant impact on expenditures
Nothing to Report.

Significant changes in use or care of human subjects, vertebrate animals, biohazards, and/or select agents
Nothing to Report.

Significant changes in use or care of human subjects
Nothing to Report.

Significant changes in use or care of vertebrate animals
Nothing to Report.

Significant changes in use of biohazards and/or select agents
Nothing to Report.

6. PRODUCTS
Publications, conference papers, and presentations

Journal publications.
Peer-reviewed journal publication:
Zamani, A., Jaffe, M., Arinzeh, T. 2015. Piezoelectric Materials for Tissue Regeneration: A Review. *Acta Biomaterialia* (2015) 24:12-23. Acknowledgment of federal support - yes.

Lee, Y.S., Wu, S., Arinzeh, T., Bunge, B. Enhanced Noradrenergic Axon Regeneration into Schwann Cell-Filled PVDF-TrFE Conduits After Complete Spinal Cord Transection. *Tissue Engineering: Part A* (in revision as of 10/21/15). Acknowledgment of federal support - yes.

Books or other non-periodical, one-time publications.
Nothing to Report.

Other publications, conference papers, and presentations.
Invited Presentation and Conference Abstract:
Lee, Y.S., Wu, S., Bunge, B., Arinzeh, T*. Piezoelectric Fibrous Scaffolds for Schwann Cell Induced Spinal Cord Repair. Biomedical Engineering Society Annual Meeting, October 2014. Acknowledgment of federal support - yes. *Presenter

Conference papers:
Lee, Y.S., Wu, S., Arinzeh, T., Bunge, M. Schwann cell-laden PVDF-TrFE Conduits for Spinal Cord Repair. World Congress of Biomaterials, May 2016 (submitted). Acknowledgment of federal support - yes.

Wu, S., Lee, Y-S, Bunge, B., Arinzeh, T. Investigating Schwann Cell Growth and Neurite Extension on PVDF-TrFE Scaffolds in Vitro. World Congress of Biomaterials, May 2016 (submitted). Acknowledgment of federal support - yes.

Website(s) or other Internet site(s)

Nothing to Report.

Technologies or techniques
Nothing to Report.

Inventions, patent applications, and /or licenses
Nothing to Report.

Other products
Nothing to Report.

7. PARTICIPANTS & OTHER COLLABORATING ORGANIZATIONS

What individuals have worked on the project?

Name: Treena Arinzeh
Project Role: PI
Nearest person month worked: 3
Contribution to Project: Dr. Arinzeh oversees all aspects of the experiments in the project, determines study designs, works with collaborators, interprets data and presents and publishes findings.

Name: Mary Bunge
Project Role: Qualified Collaborator/Co-I
Nearest person month worked: 2
Contribution to Project: She oversees all in vivo experiments using the complete transection model and collaborates on the in vitro studies. She determines study designs in collaboration with the PI, interprets data and contributes to the publishing and presenting of the findings.

Name: Mesut Sahin
Project Role: Collaborator/Co-I
Nearest person month worked: 1
Contribution to Project: He oversees the in vivo experiments measuring the electrical activity of the piezoelectric materials. He determines the recording device/setup and interprets the data in collaboration with the PI.

Name: Yee-Shuan Lee
Project Role: Postdoctoral Fellow
Nearest person month worked: 12
Contribution to Project: She performs all in vivo experiments using the complete transection model and analyses.

Name: Siliang Wu
Project Role: PhD student
Nearest person month worked: 12
Contribution to Project: He performs all in vitro experiments, including materials characterization and SC cell viability and growth studies.

Name: Sinan Gok
Project Role: PhD student

Nearest person month worked: 6
Contribution to Project: He performs the piezoelectric characterization of the material in vitro and vivo.

Has there been a change in the active other support of the PD/PI(s) or senior/key personnel since the last reporting period?
Nothing to Report.

What other organizations were involved as partners?
Nothing to Report.

8. SPECIAL REPORTING REQUIREMENTS

Collaborative awards: Not Applicable

Quad Charts – Not Applicable

9. APPENDICES

Zamani, A., Jaffe, M., Arinzeh, T. 2015. Piezoelectric Materials for Tissue Regeneration: A Review. *Acta Biomaterialia* (2015) 24:12-23. Acknowledgment of federal support - yes.

Acta Biomaterialia 24 (2015) 12–23

Contents lists available at ScienceDirect

Acta Biomaterialia

journal homepage: www.elsevier.com/locate/actabiomat

Review article

Piezoelectric materials for tissue regeneration: A review

Amir Hossein Rajabi, Michael Jaffe, Treena Livingston Arinzeh *

Department of Biomedical Engineering, New Jersey Institute of Technology, Newark, NJ 07102-1982, USA

ARTICLE INFO

Article history:
Received 6 March 2015
Received in revised form 11 June 2015
Accepted 6 July 2015
Available online 7 July 2015

Keywords:
Piezoelectric
Electrical stimulation
Tissue engineering
Tissue regeneration
Scaffolds

ABSTRACT

The discovery of piezoelectricity, endogenous electric fields and transmembrane potentials in biological tissues raised the question whether or not electric fields play an important role in cell function. It has kindled research and the development of technologies in emulating biological electricity for tissue regeneration. Promising effects of electrical stimulation on cell growth and differentiation and tissue growth has led to interest in using piezoelectric scaffolds for tissue repair. Piezoelectric materials can generate electrical activity when deformed. Hence, an external source to apply electrical stimulation or implantation of electrodes is not needed. Various piezoelectric materials have been employed for different tissue repair applications, particularly in bone repair, where charges induced by mechanical stress can enhance bone formation; and in neural tissue engineering, in which electric pulses can stimulate neurite directional outgrowth to fill gaps in nervous tissue injuries. In this review, a summary of piezoelectricity in different biological tissues, mechanisms through which electrical stimulation may affect cellular response, and recent advances in the fabrication and application of piezoelectric scaffolds will be discussed.

Statement of Significance

The discovery of piezoelectricity, endogenous electric fields and transmembrane potentials in biological tissues has kindled research and the development of technologies using electrical stimulation for tissue regeneration. Piezoelectric materials generate electrical activity in response to deformations and allow for the delivery of an electrical stimulus without the need for an external power source. As a scaffold for tissue engineering, growing interest exists due to its potential of providing electrical stimulation to cells to promote tissue formation. In this review, we cover the discovery of piezoelectricity in biological tissues, its connection to streaming potentials, biological response to electrical stimulation and commonly used piezoelectric materials for tissue regeneration. This review summarizes their potential as a promising scaffold in the tissue engineering field.

1. Introduction

Piezoelectric materials are smart materials that can generate electrical activity in response to minute deformations. First discovered by Pierre and Jacques Curie in 1880 [1], deformation results in the asymmetric shift of ions or charges in piezoelectric materials, which induces a change in the electric polarization, and thus electricity is generated. Piezoelectric materials are widely used in various electronic applications such as transducers, sensors and actuators. For biomedical applications, piezoelectric materials allow for the delivery of an electrical stimulus without the need for an external power source. As a scaffold for tissue engineering, there is growing interest in piezoelectric materials due to their potential of providing electrical stimulation to cells to promote tissue formation. In this review, we cover the discovery of piezoelectricity in biological tissues, its connection to streaming potentials, biological response to electrical stimulation and commonly used piezoelectric materials for tissue regeneration. This review summarizes their potential as a promising scaffold in the tissue engineering field.

2. Piezoelectricity in biological tissues

In 1940, Martin [2] noticed the first demonstration of biological piezoelectricity, when he detected electric potentials from a bundle of wool encapsulated in shellac while compressed by two brass plates. The main constituent of mammalian hair, wool, horn and hoof is α-keratin [3,4], which has a spiral α-helix structure [4].

* Corresponding author at: Biomedical Engineering, New Jersey Institute of Technology, 323 Martin Luther King Blvd., Newark, NJ 07102, USA.
E-mail address: arinzeh@njit.edu (T.L. Arinzeh).

http://dx.doi.org/10.1016/j.actbio.2015.07.010
1742-7061/

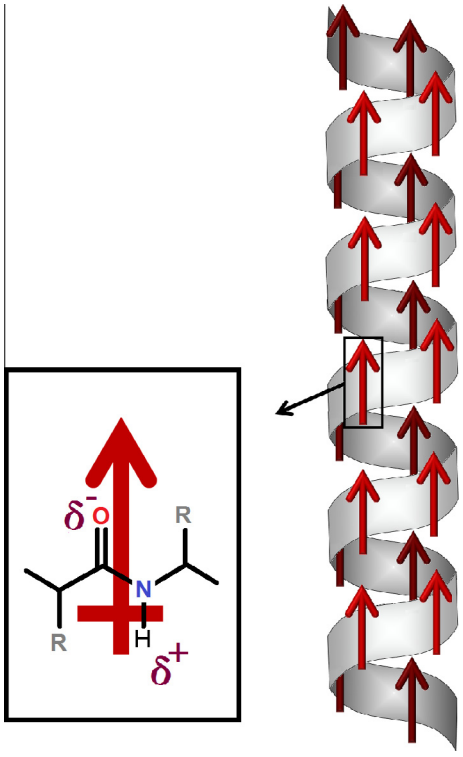

Fig. 1. Schematic illustration of permanent polarization in α-helix. Red arrows demonstrate the direction of the dipole moment. (For interpretation of the references to colour in this figure legend, the reader is referred to the web version of this article.)

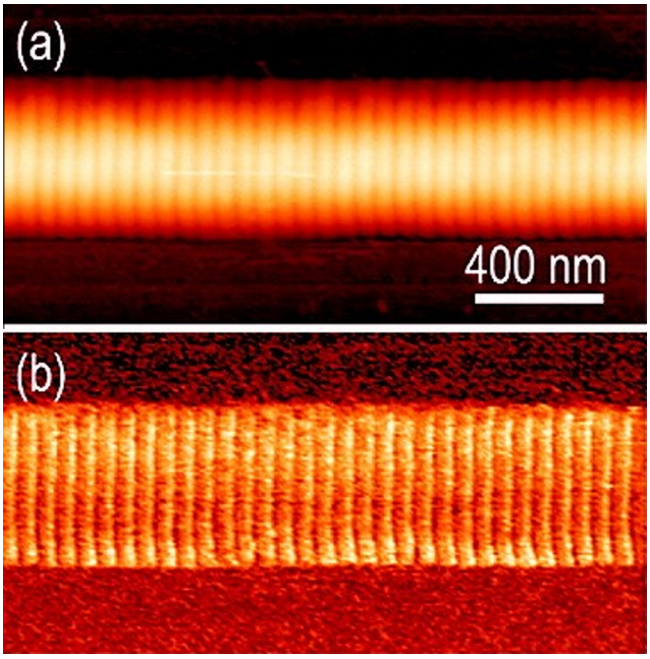

Fig. 2. Topography of a single collagen fibril imaged by atomic force microscopy (a), and the amplitude of its corresponding shear piezoelectricity acquired by piezoforce microscopy in the lateral mode (b) [16].

The piezoelectricity of such tissues is attributed to the compact alignment of these highly ordered α-helices and their inherent polarization [5,6]. α-Helix is a right handed coil stabilized by the hydrogen bonds between the hydrogen of one amine group with the oxygen of a consecutive carbonyl group. As demonstrated in Fig. 1, the helical structure repeatedly aligns the dipoles of the backbone amino acids and causes a significant permanent polarization [7,8].

Yasuda [9] reported the piezoelectricity of bone in 1954. Later, Yasuda and Fukada [10] observed piezoelectricity in boiled bone and consequently concluded that living cells were not responsible for the piezoelectric response. They attributed the piezoelectric behavior of bone to the application of shear on collagen. Bone is a composite of densely packed aligned collagen fibrils containing hydroxyapatite particles [11]. Collagen as the most abundant mammalian protein, also has a spiral structure consisting of three helices, called triple helix [12]. Piezoforce microscopy (PFM) is a modification of atomic force microscopy (AFM), which has been recently used to study the piezoelectricity of nanomaterials. An AC bias between the conductive AFM tip and the substrate beneath the sample applies an electric field through the sample, causing a deformation in the piezoelectric material. The contacting AFM tip detects the deformation, which is subsequently translated to the amplitude of the piezoresponse [13]. PFM can be performed in vertical or lateral modes; vertical deflection of the AFM tip manifests normal deformation of the material. In lateral mode, torsion of the AFM tip reveals shear deformation of the domain [14].

The piezoelectricity of single collagen fibrils has been studied using piezoforce microscopy [15,16]. PFM images of collagen fibrils show lateral piezoresponse along the fibril axis and negligible vertical and radial piezoresponse, revealing the unidirectional polarization along the collagen fibril axis [15]. Fig. 2 shows the topography of a single collagen fibril imaged by AFM, and its corresponding shear piezoelectricity imaged by lateral PFM, demonstrating the periodicity of the piezoforce amplitude attributed to the gaps and overlaps in the quarter-staggered structure of collagen [16].

For years, it was believed that since hydroxyapatite crystalizes in a centrosymmetric space group in the hexagonal system [17], it could not be piezoelectric [18]. However, computational studies reported a lack of an inversion center in hydroxyapatite that could theoretically suggest possible piezoelectricity of this crystal [19]. Tofail et al. [20] have demonstrated the piezoelectricity of sintered hydroxyapatite using PFM, which suggests that alongside collagen, hydroxyapatite may also contribute to the piezoelectricity of bone. Piezoelectricity of other collagenous tissues such as tendon [21–23], dentin [24], cementum [25] and cartilage [26,27] have also been reported. Polysaccharides such as wood [28] and chitin [29] as well as polynucleotides such as deoxyribonucleic acid (DNA) have also revealed piezoelectric response [30].

3. Piezoelectricity and streaming potential

In 1892, Julius Wolff [31] suggested that bone remodels its architecture in response to stress. "Wolff's Law" manifests itself in the denser bone in tennis players' racket-holding arms or bone loss in astronauts. After the discovery of piezoresponse in dry bone [9], the proposed mechanism to describe bone growth and resorption in response to stress was piezoelectricity. As one of the pioneers of investigating the biological effects of piezoelectricity, Bassett [32] observed that unlike undeformed samples, periodically deformed cultivated chick embryonic tibiae produced large periosteal chondroid masses after 7 days, and described Wolff's law as a negative feedback loop: applied load on bone causes strain in less dense regions; while denser and consequently stiffer regions remain unstrained. The strain is transformed into an electric field that aggregates and aligns macromolecules and ions in the extracellular matrix, which stimulates cells to remodel the bone architecture until the signal is switched off. As piezoelectric measurements expanded to wet bone [33] and wet collagen [34],

which is hydrated bone and collagen to simulate physiological conditions, dissimilarities were observed in the amplitude and behavior of the stress generated potentials between wet and dry samples. The induced electric potential was found to be dependent on the strain rate and more importantly, the relaxation time of the induced potential was much higher in wet samples. To justify the inconsistency, different hypotheses were proposed such as the p–n junction characteristic of apatite-collagen [35], which suggested bone was piezoelectric in one direction and piezoresistive in another. However, a notion that drew more recognition proposed that while piezoelectricity was accountable for stress induced potentials in dry bone, the mechanism responsible for wet bone was streaming potential [36,37]. Streaming potential theory suggested that the stress-generated potential in wet bone was due to the flow of ion-containing interstitial fluid through bone as a result of pressure. Streaming potential theory dominated after Pollack et al. [38] reported that the conductivity of the saturating fluid was significantly influential on the amplitude and polarity of the generated potentials and the longer relaxation time was due to the viscosity of the fluid. A newer theory of mechanosensation in bone suggests that the applied stress on bone is translated into biochemical signals by flowing interstitial fluid in the canaliculi-lacunae space and supplying bone cells with nutrients as well as conveying shear stress to cells [39]. In spite of the new theories, the debate exists whether one can entirely exclude piezoelectricity from mechanosensation. As illustrated in Fig. 3, Ahn and Grodzinsky [40] suggest that piezoelectricity increases the surface charge density of collagen fibers and consequently increases the zeta potential, which intensifies the streaming potential as the following equation [38]:

$$V = \frac{\zeta P \kappa}{4\pi\sigma\eta}$$

where ζ, P, κ, σ and η are the zeta potential, the pressure on the bone, the dielectric permittivity, conductivity and viscosity of the interstitial fluid, respectively. Remarkably, they support their hypothesis by recalling the piezoelectric coefficients previously reported by Anderson et al. that showed while the largest piezoelectric coefficients in dry bone were in the lateral axes, immersing the same bone in saline solution resulted in the largest piezoelectric coefficients in the longitudinal axis. This suggests that when placed in a saline solution, the electricity produced on the lateral surfaces due to piezoelectricity can be translated to zeta potential and consequently contribute to higher streaming potential along the longitudinal axis of bone [40].

4. Cellular response to electrical stimulation

In addition to piezoelectricity and streaming potentials in bone and other fibrous tissues, endogenous electric fields up to 500 mV/mm have been reported in living tissues [41]. The transport of ionic species and macromolecules associated with endogenous electric fields play crucial roles in embryonic development [42], wound healing [43] and neural regeneration [44]. There exists a difference in intracellular and extracellular ionic concentrations, resulting in a transmembrane potential of −10 to −90 mV in different types of cells. Shifts in transmembrane potential is known to alter cellular proliferation and differentiation [45], and exciting the resting transmembrane potential in neurons can trigger self-propagation of action potential along the axon [46].

This vital role of electricity in living systems have inspired numerous investigations to either mimic biological piezoelectricity and endogenous electric fields or manipulate transmembrane potentials by external electrical stimulation to enhance cellular growth and differentiation. The attention in neural regeneration has been drawn to repairing peripheral nerve injuries through improved neural differentiation and directional outgrowth of neurites. Direct electric fields as low as 70 mV/mm have shown to facilitate the outgrowth of the neurites of embryonic chick dorsal

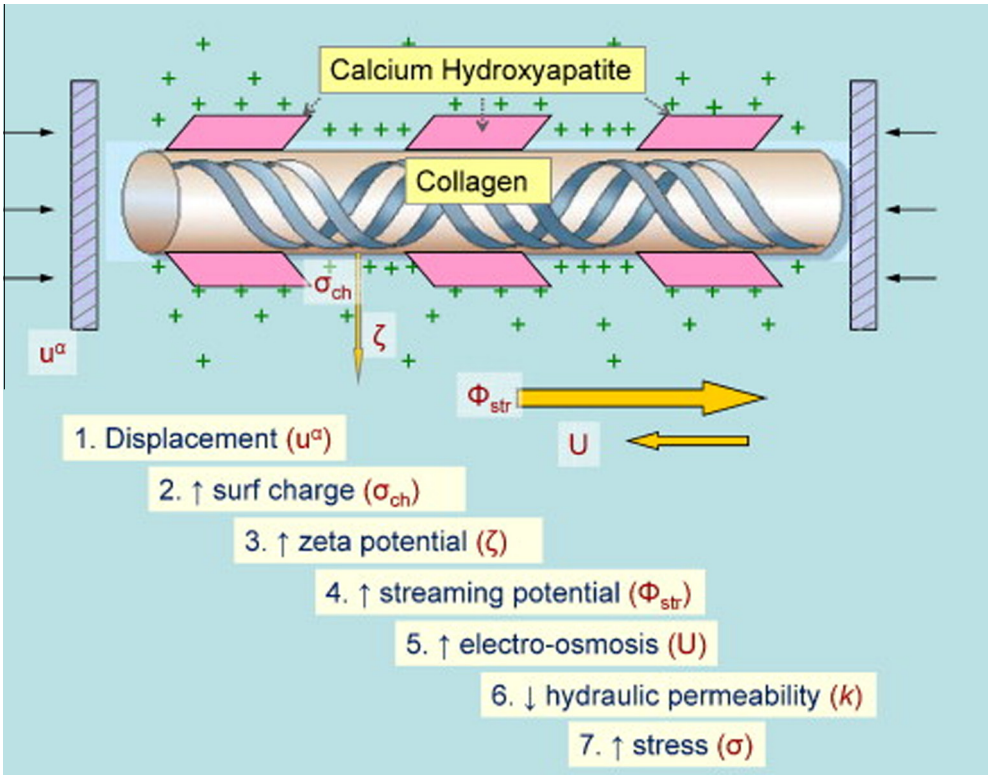

Fig. 3. Ahn and Grodzinsky's hypothesized model illustrating how applied stress on bone results in greater surface charges, which consequently increases zeta potential, streaming potential, electroosmosis and dynamic stiffness as well as decreases hydraulic permeability in the open-circuit condition [40].

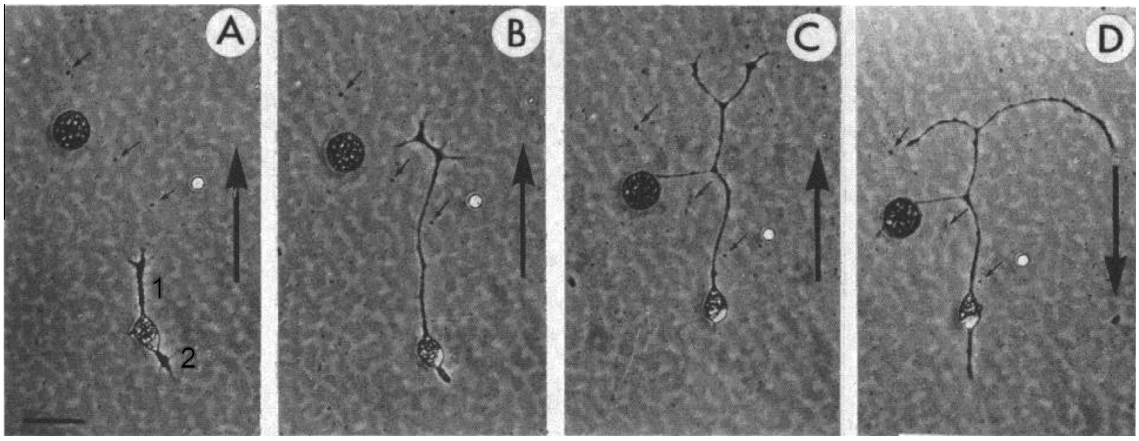

Fig. 4. Direction and outgrowth of the neurites (labeled 1 and 2) of a bipolar neuron as a result of stimulation by a 500 mV/mm electric field. The black arrow shows the direction of the electric field. The neuron at the beginning of the electrical stimulation (A); after 2 h of exposure to the electric field, neurite 1 has noticeably grown towards the cathode (B); 4 h of stimulation in the same direction resulted in further extension of neurite 1 as well as its branching, while neurite 2 has almost diminished (C); 2 h after changing the direction of the electric field, the tips of neurite 1 curved and neurite 2 grew towards the new cathode (D) [48].

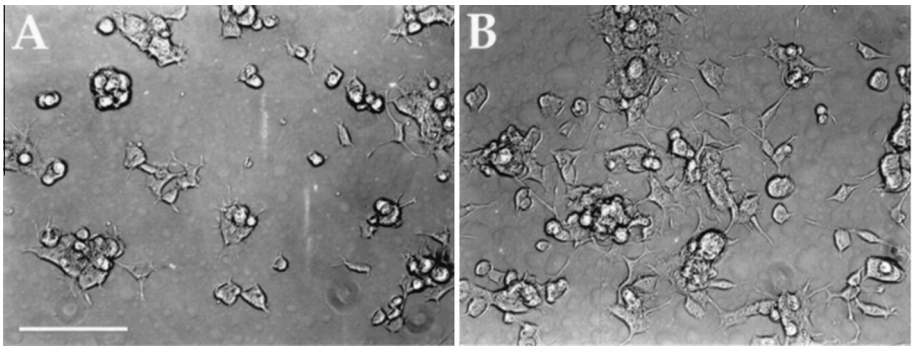

Fig. 5. Differentiation of PC-12 cells on PPy films without (A) and with (B) the application of 100 mV across the film. The scale bar is 100 μm [55].

root ganglions (DRG) toward the cathode [47]. Applying a direct electric field of 250 mV/mm or higher on Xenopus neurons resulted in more neurite-bearing cells with longer neurites directed towards the cathode and contracted neurites on the anode side (Fig. 4) [48]. Promising results are not limited to neurons; an early study on the effect of electrical stimulation on bone formation showed that implanting insulated batteries in the medullary canal of canine femora caused substantial formation of endosteum near the cathode in a 14–21 day period [49]. Even in the absence of external electrical stimulation, implanting poled sintered hydroxyapatite disks in canine cortical bone resulted in the filling of a 0.2 mm gap between the negatively charged hydroxyapatite surface and the cortical bone in 14 days, while no bone formation occurred using the unpoled hydroxyapatite before day 28 [50].

Electrical stimulation can be applied through the substrate or the medium. While DC electrical stimulation through media aligns Schwann cells perpendicular to the direction of the electric field, AC electric field through the media changes the cellular morphology from bipolar spindles to flat and spread with more processes [51]. Applying currents through conductive polymers such as polypyrrole (PPy) and polyaniline (PANi) has been an alternative method for electrical stimulation. Even without electric current, cells have shown favorable extension and proliferation on substrates consisting of conductive polymers in comparison with control samples [52–54]. Fig. 5 shows how applying a direct electric potential of 100 mV across PPy film almost doubled the length of neurites of PC-12 cells in comparison with the unstimulated films [55]. Applying a direct current of 10 μA through PPy films also triggered significantly higher adsorption of fibronectin (FN) onto the surface, specifically in highly concentrated FN solutions and at early stages of exposure. The PC-12 cells seeded on these films grew up to 50% longer neurites than on unstimulated films [56]. As an approach towards incorporating three-dimensional (3D) features of fibrous scaffolds and electrical stimulation, Schmidt et al. [57] applied a direct electric field of 100 mV/mm through an electrospun 3D scaffold coated with PPy, and observed significant improvement in the number of neurite-bearing PC-12 cells and their neurite lengths.

Another method to construct 3D conductive scaffolds is electrospinning blends of nonconductive and conductive polymers. Direct electrical stimulation of electrospun composites of 30 wt.% PANi and poly(L-lactide-co-ε-caprolactone) copolymer with 20 mA increased the proliferation of NIH-3T3 fibroblasts [54]. Neural stem cells seeded on nanofibrous scaffolds composed of poly(ε-caprolactone) (PCL), gelatin and 15 wt.% PANi also showed significantly higher proliferation as well as growing longer neurites in response to one hour of direct electrical stimulation of 100 mV/mm [58]. Electrospun scaffolds composed of PANi and poly-L-lactic acid also increased the neurite lengths of C17.2 rat stem neural stem cells when stimulated with 100 mV/mm [53]. In most direct electrical stimulation studies, there is an optimum electric field in the range of endogenous electric fields or transmembrane potential, over which there is either no significant improvement [57] or the field is detrimental to the cells [52,54].

Alternating electric fields also have been investigated. Alternating electric fields have shown to cause morphological

changes and significantly increased number of processes in Schwann cells, but did not lead to directional outgrowth [51]. Since endogenous electric fields and transmembrane potentials are direct rather than alternating, many neural studies use direct electrical stimulation. On the contrary, the periodic nature of the stress applied to bone has inspired investigations in bone repair to focus on alternating electric fields to enhance osteoblast proliferation and activity. Moreover, in order to avoid electrode implantation and consequently electrolytic byproducts, noninvasive stimulation for bone fracture healing drew widespread attention. Noninvasive bone growth stimulators are approved by the U.S. Food and Drug Administration (FDA) [59,60], and are currently marketed for healing fractures and nonunions. In research, techniques implemented for osteogenic electrical stimulation varies from capacitively coupled stimulation [61–63], to applying electromagnetic waves using Helmholtz [64–66] and solenoid coils [67,68]. Capacitively coupled electrical stimulation have shown to significantly increase the proliferation [61] and matrix mineralization of osteoblast-like cells [63].

The mechanisms through which electrical stimulation causes cellular migration and alters proliferation and differentiation are not yet fully understood. It is speculated that the electric field effect is either direct by intracellular components such as ions, growth factors and receptors, or indirect by agglomeration or conformational change of extracellular ions and proteins [48,55]. Free calcium cations (Ca^{2+}) are considered a major factor in both direct and indirect mechanisms of electrical stimulation. Electric fields redistribute Ca^{2+} in the extracellular matrix or on the substrate [51]. Intracellular Ca^{2+} concentrations are also reported to increase due to electrical stimulation [69]. Fig. 6 illustrates an adaptation of the galvanotaxis of cells as reviewed by Mycielska et al. [41]. Direct electric field depolarizes the cathodal side of the cell and hyperpolarizes the anodal side. This leads to the diffusion of extracellular Ca^{2+} through the anodal side into the cell. Increase in the Ca^{2+} may cause actin depolymerization and consequently contraction on the anodal side, which pushes the cell forward and thus makes the cathodal side of the cell protrude [41]. This could explain the phenomenon observed by Patel and Poo [48] as shown in Fig. 4, i.e. the outgrowth of the neurites on the cathodal side of the cell and the diminishing of the neurites on the anodal side. Patel and Poo, on the other hand, found that neither blocking Na^{+} channels nor nullifying intercellular Ca^{2+} gradient stopped directional neurite outgrowth in cells exposed to direct electric field [48]. However, there was a larger distribution of concanavalin A receptors on the cathodal side of the cell than on the anodal side, which made them conclude that the effect of electrical stimulation on directional growth of neurons could be direct by preferential migration of membrane receptors [48]. Schmidt et al. reported that electrical stimulation could result in more favorable conformational changes in fibronectin, which facilitated the adsorption of more proteins onto the biomaterial [56]. Since some extracellular matrix proteins play critical roles in cellular attachment, more adhered proteins on the surface could improve cellular adhesion and outgrowth.

The effect of electrical stimulation on enhanced bone formation was initially based on the indirect hypothesis; piezoelectricity of bone generated electric fields that aggregated charged ions and macromolecules in the bone interstitial fluid, which resulted in enhanced osteoblast activity [32]. Direct electric fields are assumed to mobilize Ca^{2+} and Mg^{2+} towards the cathode or negatively charged surface and cause apatite formation, which can become a scaffold for bone formation by osteoblasts [50,70]. Increased levels of gene expression for bone morphogenic proteins (BMP-2 and -4) as a result of electromagnetic stimulation were noted [66]. Zhuang et al. [61] also found that capacitively coupled electrical stimulation increased TGF-β1 gene expression as well as the proliferation of osteoblasts. TGF-β1 expression was modulated by the calcium–calmodulin pathway.

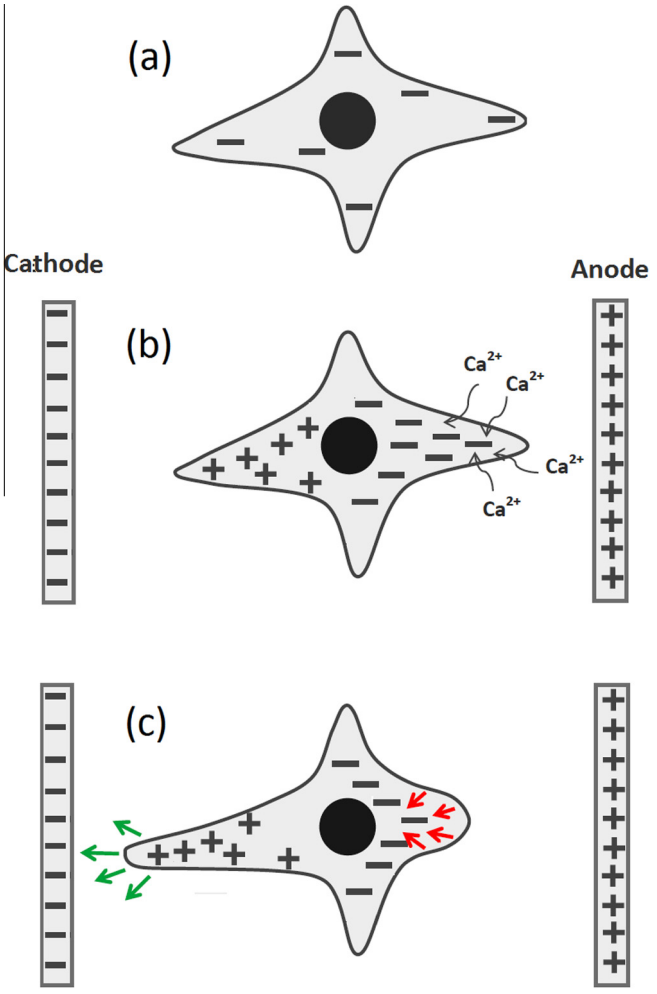

Fig. 6. A cell with insignificant voltage-gated Ca^{2+} channels at resting transmembrane potential (a); application of a direct electric field redistributes the intracellular charges resulting in the depolarization and hyperpolarization of the cathodal and anodal sides of the cell, respectively. Extracellular Ca^{2+} is consequently diffused through the anodal side (b). The increase in the intracellular Ca^{2+} on the anodal side depolymerizes actin. The result is the contraction of the anodal side and protrusion of the cathodal side (c) (adapted from Mycielska et al. [41]).

5. Piezoelectric materials in tissue regeneration applications

5.1. Piezoceramics

Using piezoelectric materials as tissue engineering scaffolds enables electrical stimulation without the need for electrodes, external source of electricity or implanting batteries, which also eliminates the chance of accumulating products of electrolysis. Piezoelectric scaffolds can generate electric pulses as a result of transient deformations, which can be imposed by attachment and migration of cells or body movements. The materials used in scaffolds needs to be biocompatible and possess reasonable piezoelectric coefficients. The most commonly used piezoelectric material in electronics is lead zirconate titanate (PZT) [71] owing to its notable piezoelectric and electromechanical coupling coefficients. PZT has been used to build a wirelessly powered nerve-cuff, in which the implanted piezoceramic was deformed by ultrasound radiated through the skin, and consequently generated electric

pulses that could cause muscle-twitch in a rat's hind limb [72]. In another study, rat cortical neurons cultured on PZT slides coated with poly-L-lysine grew significantly longer axons, despite a decrease in cell number. Also the frequency and amplitude of the excitatory postsynaptic currents increased, suggesting that piezoelectricity could have augmented neuronal activity [73]. Nevertheless, 60 wt.% of PZT is lead, which even in low doses causes serious health problems such as neurotoxicity [74], pregnancy complications [75], attention deficit hyperactivity [76] and slow growth rate in children [77]. There have been efforts to replace PZT with lead-free piezoceramics. Among popular lead-free piezoceramics, zinc oxide (ZnO), barium titanate (BT), potassium sodium niobate (KNN), lithium sodium potassium niobate (LNKN), and boron nitride nanotubes (BNNT) have substantial piezoelectric coefficients. One major concern about using piezoceramics in tissue engineering is the cytotoxicity of these materials. Most piezoelectric ceramics, such as PZT [78], ZnO [79], BT [80], KNN and LNKN [81], exhibit ion dissolution in biological fluids. While some of the released ions for instance Pb^{2+} could be toxic, others could be relatively safe or even favorable at low doses [82] and cytotoxic at higher concentrations [83]. Therefore, in some studies involving piezoceramics, the piezoelectric particles are embedded in polymer [82,84,85] or ceramic [86–88] matrix composites to control ion dissolution. Although BNNTs are highly stable in aqueous solutions, their cytotoxicity is still of controversy [89–92]. Composites of ZnO nanoparticles in polyurethane have been employed to engineer neural tissues, which resulted in lower density of astrocytes as ZnO increased, particularly on composites with more than 10%ZnO. This was attributed to the increase in surface energy of the composites as a result of the increase in ZnO, which could alter both adsorption and conformation of extracellular matrix proteins on the surface. Findings were particularly noteworthy because the accumulation of astrocytes on an implant results in glial scars, which can hinder neural regeneration [84]. Electrospun fibrous composite scaffolds made of ZnO particles and polyurethane (PU) resulted in improved attachment and proliferation of mouse fibroblasts on the composite scaffolds in comparison to pure PU scaffolds [85].

Barium titanate (BT) was the first lead-free piezoceramic that was investigated in bone repair. Initial results were promising: BT cylinders implanted in canine femora formed a strong interfacial bond with bone. However, no significant difference was observed between poled/piezoelectric BT implants and the unpoled ones [93]. Further in vivo studies using this piezoceramic were composites of hydroxyapatite (HA) and BT where results showed new bone formation on the BT/HA implant after just one week, while bone did not grow on HA implant until two weeks. Interestingly, bone formation was dependent on the direction of implantation (vertical or horizontal), which could indicate the possible role of piezoelectric coefficients in different directions [87]. The proliferation and attachment of human osteosarcoma cells on both poled and unpoled HA-90%BT composite versus pure HA disks revealed no significant difference in vitro, possibly because the experiments took place in static conditions [86]. Similarly in a more recent study, fibroblasts on freeze-cast BT/HA composites showed no cytotoxicity, and the highest cell number was observed on HA-70%BT, compared with HA-90%BT and HA-50%BT [88]. Adding BT nanoparticles to electrospun PCL scaffolds also increased osteocalcin gene expression of pre-osteoblasts [82]. Attachment and internalization of glycol-chitosan coated BT nanoparticles to the cell membrane and even in the cytoplasm of mesenchymal stem cells significantly altered the conformation of the cytoskeleton and increased the stiffness of the cells, which resulted in enhanced osteogenic differentiation [94].

Potassium sodium niobate (KNN) and lithium sodium potassium niobate (LNKN) are two other lead-free piezoceramics with piezoelectric coefficients of almost two orders of magnitude larger than natural bone, whose cytotoxicities have been evaluated. The viability of mouse fibroblasts cultured on KNN and LNKN powders for 24 h were respectively 84% and 58%, although the value for LNKN could be improved to 72% by adjusting the pH. The slightly higher toxicity of LNKN could be due to the release of Li^+ in the media after immersion of the piezoceramic [81]. In another study, rat osteoblasts showed better attachment and proliferation on the negatively charged surface of the poled LNKN porous scaffolds than unpoled scaffolds [95].

In a novel approach, Ciafoni et al. [96] internalized boron nitride nanotubes (BNNT) inside the cytoplasmic vesicles of PC-12 cells and wirelessly agitated the piezoelectric nanotubes by external ultrasound. Their results showed that neurite lengths as well as the number of neurites per differentiated cell were significantly greater in cultures with BNNTs followed by ultrasound agitation. Interestingly, they also observed that blocking calcium channels diminished the response to stimulation, suggesting that electrical stimulation contributes to differentiation through calcium signaling pathways.

5.2. Piezopolymers

Discovery of the piezoelectricity of polyvinylidene fluoride (PVDF) by Kawai [97] made this polymer a candidate substitute for PZT. Due to its flexibility and nontoxicity [98], PVDF has been used for a variety of biomedical applications, from tissue engineering scaffolds to implantable self-powered devices [99]. PVDF crystalizes in various phases. α-PVDF has a trans-gauche conformation without a net dipole moment and is nonpiezoeletric (Fig. 7(a)). β-PVDF, however, has all-trans conformation, which exhibits a net dipole moment and is thus piezoelectric [100] (Fig. 7(b)). Alternatively, poly[(vinylidenefluoride-co-trifluoroethylene] (PVDF-TrFE) is a copolymer with all-trans conformation, piezoelectricity and high electromechanical coupling coefficient [101] (Fig. 7(c)).

Valentini et al. [102] used PVDF to build guidance channels for neural regeneration. They employed mechanical stretching to orient the dipoles and transform α-PVDF to β-PVDF, followed by electric poling in order to fix the dipoles and achieve piezoelectric tubes to be used as sciatic nerve guidance channels to treat rat sciatic nerves with 4 mm gaps. After 4 weeks of implantation, the numbers of myelinated axons in the midpoint of the piezoelectric tubes were significantly higher than the control tubes. In a

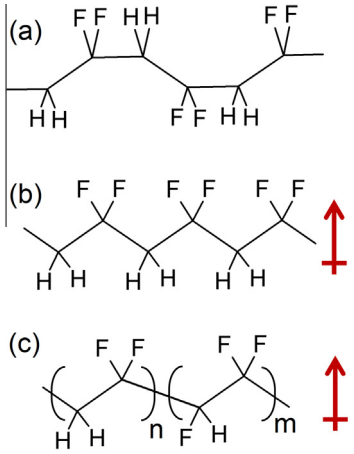

Fig. 7. Chemical structures of α-PVDF with trans-Gauche conformation and no net dipole moment (a); β-PVDF with all-trans conformation having a net dipole moment (b); and PVDF-TrFE copolymer with an inherent net dipole moment (c).

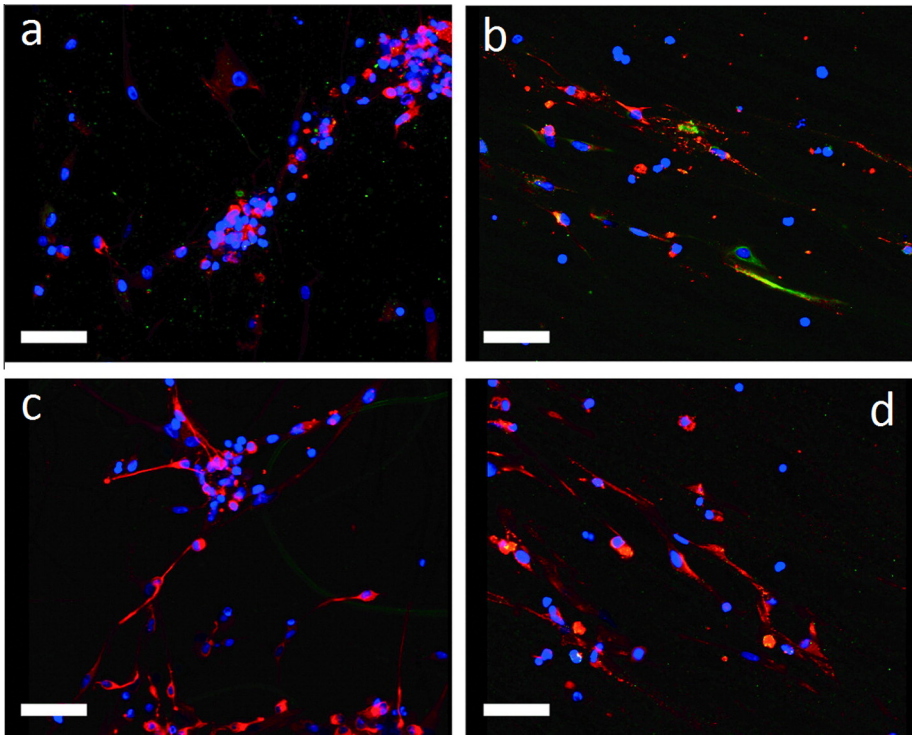

Fig. 8. Confocal fluorescent microscopic images of the cells cultured in induction media on electrospun microfibrous PVDF-TrFE unannealed random (a), unannealed aligned (b), annealed random (c) and annealed aligned (d) scaffolds after 9 days. Anti-nestin (green), anti-β-III tubulin (red), anti-GFAP (blue), and counterstained with DAPI (blue) [107]. (For interpretation of the references to colour in this figure legend, the reader is referred to the web version of this article.)

following investigation, Valentini et al. [103] repeated the experiment with piezoelectric PVDF-TrFE to avoid stretching. They poled two groups to have negatively charged and positively charged nerve guidance channels as well as an unpoled group. The positively poled tube led to the most myelinated axons in the regenerated nerves bridging the 10 mm gaps after 4 weeks, while negatively poled and unpoled tubes resulted in the intermediate and the fewest number of myelinated axons, respectively. Valentini et al. [104] also studied the differentiation of mouse neuroblastoma cells on poled and unpoled PVDF substrate after 24–96 h and found that despite similar chemical and topographical properties of the piezoelectric and nonpiezoelectric substrates, the former resulted in significantly enhanced neurite outgrowth and extension.

In a series of studies, Arinzeh et al. [105–108] used electrospinning to construct fibrous piezoelectric scaffolds for neural and bone tissue engineering. Electrospun PVDF-TrFE fibrous scaffolds showed higher crystallinity and β-phase content as compared to the starting powder material. In a study establishing cytocompability, metabolic activity and gene expression of the cultured human dermal fibroblasts suggested adequate cellular proliferation and attachment on the PVDF-TrFE fibrous scaffolds during a 7 day period. Results were not significantly different from tissue culture plates as the control group. However, since plasma treated polystyrene used in tissue culture plates are favorable sites for the attachment and growth of anchorage-dependent cells such as fibroblasts, the comparability between the two groups suggested the cytocompatibility of the piezoelectric fibers [105]. In a subsequent study, electrospun PVDF and PVDF-TrFE fibrous scaffolds were used to examine neurite outgrowth using dorsal root ganglions (DRGs). Results showed that while neurites attached and extended on PVDF and PVDF-TrFE fibrous scaffolds, their attachment and extension on films casted from the same materials were poor, which suggested the 3-D fibrous environment facilitated neurite outgrowth. Measurement of average neurite lengths and the aspect ratio of the DRGs after 4 days of cell culture showed there was a linear relationship between fiber diameter and fiber alignment with neurite extension and directionality of the DRGs. Annealing the electrospun mats at 135 °C for 96 h increased the crystallinity and piezoelectric crystal phase content in the PVDF-TrFE scaffolds. Longest DRG neurite lengths were observed on annealed aligned PVDF-TrFE microfibrous scaffolds. In addition, fiber alignment had a dominant impact on neurite extension. Regardless of fiber diameter, alignment resulted in a significantly lower aspect ratios of the DRGs on both PVDF and PVDF-TrFE fibrous scaffolds indicating more directional extension, while random fibrous scaffolds resulted in radial neurite extension similar to the control group i.e. collagen-coated tissue culture plates [106].

Arinzeh et al. [107] investigated the differentiation of human neural stem/precursor cells (hNSC/NPC) on PVDF-TrFE fibrous scaffolds and films. Results showed that cells on electrospun piezoelectric fibrous scaffolds were mostly neuron-like β-III tubulins, while on nonpiezoelectric laminin-coated plates, mainly nestin was expressed. Fiber morphology and contact guidance, crystallinity and consequently the piezoelectricity of the PVDF-TrFE scaffolds may have accelerated the differentiation of hNSC/NPCs to neuron-like β-III tubulins. Although the cultures were performed in static conditions, the authors suggest that results may be attributed to transient surface charges generated due to minute deformation of the piezoelectric fibers by cellular attachment and migration. Fig. 8 illustrates how alignment and annealing of the microfibers resulted in longer neurite extension and enhanced differentiation of hNSC/NPCs to neuron-like cells expressing β-III tubulin, respectively. While in unannealed samples nestin stained cells are still noticeable, in annealed samples cells expressing nestin diminish and cells expressing β-III tubulin becomes dominant.

Using electrospun PVDF fibrous scaffolds to differentiate mesenchymal stem cells into osteoblasts indicated that fibers

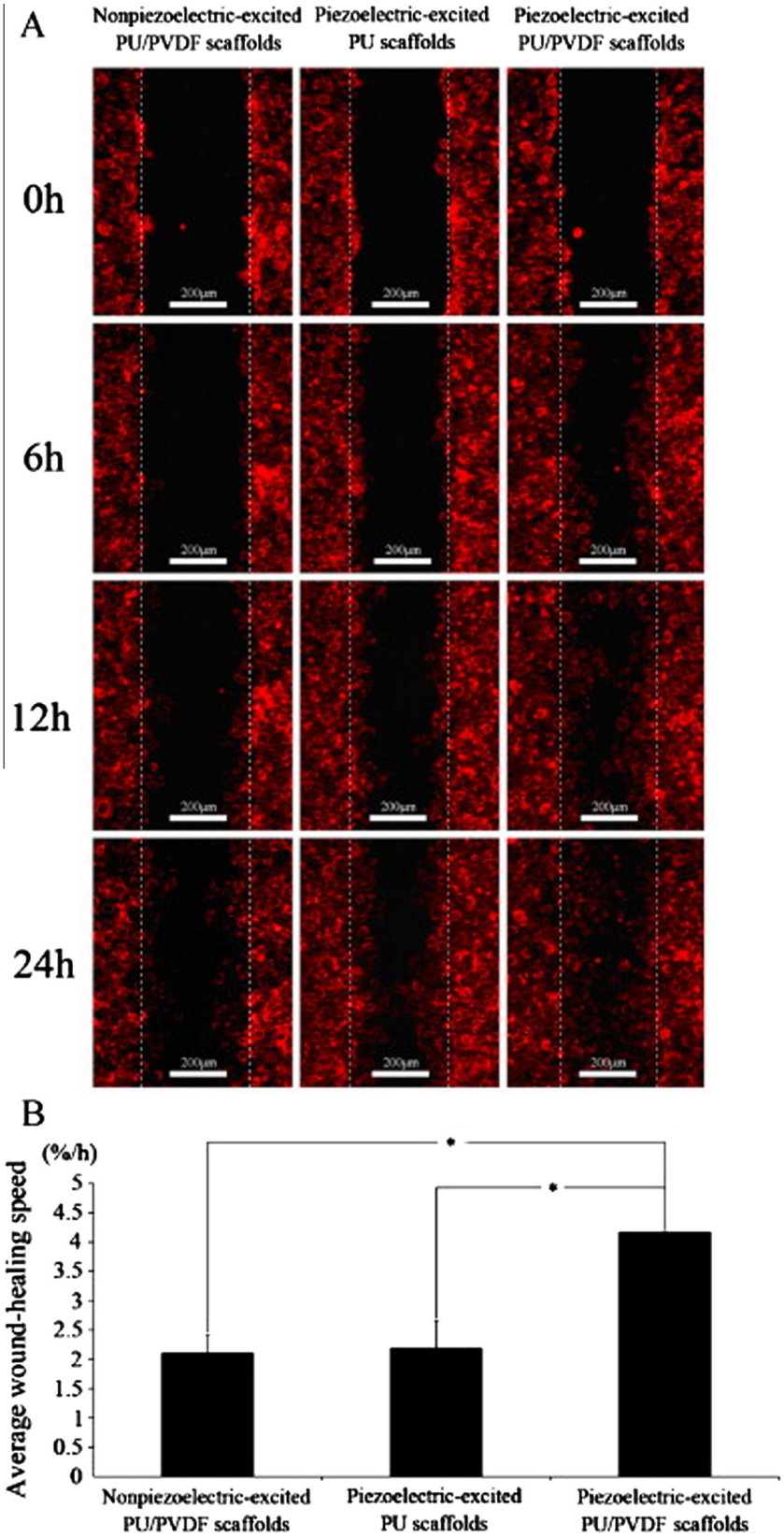

Fig. 9. Imaging of the migration of fibroblasts into the wound on undeformed PU/PVDF scaffolds, deformed PU scaffolds and deformed PVDF/PU scaffolds at different time points (A); and their average wound healing speeds from the corresponding scaffolds (B) [109].

Table 1
Summary of piezoelectric materials, their piezoelectric coefficients and applications.

Piezoelectric material	Piezoelectric coefficient (pC/N)	Applications
Bone	d_{15} = 0.1–0.3 [126]	Shear piezoelectricity of cortical bone by PFM [126]
Collagen	d_{15} = ~2 [16]	Most abundant protein in human body [12], responsible for the piezoelectricity of bone [10]
PZT	d_{33} = 225–590 [127]	Neural stimulator in vivo [72]
		Axonal growth in vitro [73]
ZnO	d_{33}^{*} = 12.4 [128]	PU/ZnO nanoparticles composite for nerve guidance channels [84]
BT	d_{33}^{**} = 191 [129]	Sintered BT in bone growth in vivo [93]
		BT/HA composite for bone growth in vivo [87]
		BT/HA composite to grow osteoblast-like cells in vitro [86]
		PCL/BT nanoparticles composite for osteogenic differentiation in vitro [82]
		BT nanoparticles for osteogenic differentiation in vitro [94]
		Porous BT/HA composites for cytotoxicity tests [88]
LNKN	d_{33} = 89 [81]	Bone growth in vitro [95]
BNNT	d_{33} = 0.3 [130]	Neural growth in vitro [96]
PVDF	d_{33}^{****} = −25 [131]	Nerve guidance channels in vivo [102]
		Neural growth in vitro [104]
		PVDF/PU composite for wound healing in vitro and in vivo [109]
		Fibronectin adsorption and cellular attachment [111]
		Bone formation in vitro [108]
		Neural growth in vitro [110]
		Osteogenic differentiation in vitro [112,113]
PVDF-TrFE	d_{33}^{***} = −25.2 [132]	Nerve guidance channels in vivo [103]
		Neural differentiation in vitro [107]
		Neural growth in vitro [106]
PLLA	d_{14} = −9.82 [133]	Bone growth in vivo [118]
		Neural differentiation and growth in vitro [121,122]
		PLLA blends for bone formation in vitro [123]
		Protein adsorption [125]
		PLLA blends for vascular differentiation in vitro [124]

* ZnO thin films.
** BT single crystals.
*** PVDF-TrFE (80:20).
**** Theoretically calculated.

electrospun at higher voltages were more favorable than lower potentials [108]. Even though tissue culture plates had the highest attachment and proliferation of mesenchymal stem cells; at early days of culture, alkaline phosphatase activity and matrix mineralization on the electrospun scaffolds were superior, particularly on scaffolds electrospun at higher electric potentials. This could be attributed to the presence of more piezoelectric β-PVDF that could have enhanced osteogenic differentiation.

Guo et al. [109] electrospun blends of polyurethane (PU) and PVDF to study the effect of piezoelectricity on wound healing and fibroblast activity. For mechanical deformation, they used culture plates with flexible bottoms that could be biaxially stretched. Having observed an increase in the piezoelectric coefficient as well as a decrease in the mechanical properties of the composite scaffolds as a result of increasing PVDF/PU ratio, they used PVDF/PU of 1 as the optimum composition for culturing mouse embryo fibroblasts. In accordance with Arinzeh et al.'s results [105,106,108], comparison of the FTIR spectra, DSC thermograms and XRD patterns of PVDF powder and electrospun PVDF/PU scaffolds showed α to β phase transformation as a result of electrospinning. As shown in Fig. 9, comparison of the wound healing rates of the fibroblasts cultured on the three groups showed that deformation of the electrospun PVDF/PU scaffolds by 8% at 0.5 Hz almost doubled the cellular migration to the scratched area after 24 h, as opposed to undeformed PVDF/PU and deformed PU scaffolds as controls. Also, the number of cells attached onto the PVDF/PU was higher than the control samples. Their results demonstrated that the enhanced migration and adhesion was due to the piezoelectric response i.e. a combination of piezoelectric scaffold and deformation and not deformation or microstructure solely. Guo et al. [109] also implanted the PVDF/PU and PU scaffolds in three rat body parts: vertex with less deformation and higher blood flow; back and abdomen with higher deformation. Histological imaging showed that in the PU group, the vertex scaffold had enhanced fibrosis compared with back or abdomen scaffolds, whereas in PVDF/PU group, the three scaffolds had similar fibrosis levels. This finding was attributed to the high deformation rate in the back and abdomen that triggered piezoelectric response from the PVDF/PU scaffold. Moreover, the levels of fibrosis in PVDF/PU scaffolds were higher than PU scaffolds in all body parts. The authors attributed these changes in the alteration of the intracellular ion channels caused by the change in the permeability of cell membranes [109].

Royo-Gascon et al. [110] extruded, stretched and poled PVDF films to build substrates for rat spinal cord neurons. To avoid the indirect effect of protein adsorption at early stages as discussed before [56], they started mechanical deformation via vibration 24 h after cell attachment. By vibrating the plates for 96 h at 50 Hz, the arborization, number of neurites, and cell density increased remarkably, while the opposite results were observed for the unpoled samples. They concluded that local calcium ion concentration as well as other second messenger molecules such as cAMP could be responsible for enhanced results caused by electrical stimulation [110].

Similar to the previously discussed fibronectin (FN) adsorption to conductive polymers with direct electric currents [56], one possible approach to explicate favorable cellular response to piezoelectric materials is enhanced protein adsorption due to static or dynamic electric charges on the surface [111,112]. Poling has shown to result in higher FN adsorption followed by increased cell numbers on β-PVDF films, possibly due to orientation of dipoles on the surface, which also manifests itself in higher hydrophilicity of poled β-PVDF samples compared to unpoled ones [111]. Both negatively and positively poled β-PVDF groups have been reported to

result in enhanced osteogenic differentiation of adipose stem cells compared to the unpoled films. Negatively poled β-PVDF films lead to round and spread cells with significantly higher focal adhesion density. This has been attributed to changes in the conformation of adsorbed FN, exposing more favorable motifs for integrin receptors to attach [113].

Unlike PVDF, Poly-L-lactic acid (PLLA) is a biodegradable [114] polymer with helical structure and accordingly permanently oriented dipoles [115,116]. The discovery of the piezoelectricity of PLLA by Fukada [117], inspired attempts to use this biocompatible and biodegradable polymer as a bone substitute with the capability to mimic the piezoelectricity of natural bone. Fukada et al. [118] implanted drawn and consequently piezoelectric PLLA rods in the intramedullary cavity of feline tibiae, and observed meaningfully higher callus formation in contrast to undrawn PLLA and polyethylene rods in a 4–8 week period. Interestingly, callus formation significantly increased as a result of increase in the draw ratio, and consequently higher piezoelectricity, which was an indication that the enhancement was due to the electricity generated through bending strain of the piezoelectric rod as a result of animal movement. Currently, PLLA is approved by the U.S. Food and Drug Administration (FDA) as a bone implant device [119,120].

Most of the research on PLLA in tissue engineering has yet focused on the versatility of producing biodegradable and biocompatible nanofibrous scaffolds, without mentioning the piezoelectric aspect. Ramakrishna et al. [121,122] have constructed fibrous PLLA scaffolds using phase separation and electrospinning to differentiate and grow neural stem-like cells. PLLA has been used as a material to incorporate other bioactive materials such as HA and collagen through electrospinning to grow human fetal osteoblasts [123] or endothelial cells derived from human mesenchymal stem cells [124]. In a more piezoelectricity-inspired approach, Barroca et al. [125] used a spin-coating technique to coat PLLA on $Pt/TiO_2/SiO_2/Si$ substrates and achieved a 300 nm thin film, which was subsequently recrystallized through heat treatment. Using PFM and a direct electric bias, the PLLA surface was locally poled. Fibronectin adsorption was studied on negatively poled, positively poled and unpoled PLLA thin films. Imaging the surface using AFM in water showed that independent of sign, significantly higher amounts of fibronectin were adsorbed on both positive and negative poled areas. The adsorbed fibronectin on poled surfaces were topographically similar to the fibronectin adsorbed on hydrophobic surfaces. Barroca et al. concluded that surface charges can alter the conformation or orientation of the adsorbed proteins, which may expose or hinder their cell-binding domains. Table 1 summarizes the abovementioned materials, their piezoelectric coefficients, and reported applications.

6. Conclusion

Electricity exists in living tissues in the form of stress-generated potentials, endogenous electric fields and transmembrane potentials. Numerous studies have been carried out on whether or not imitating these biological electric fields can enhance growth and repair. Some of these efforts have resulted in clinical trials or approved medical treatments. Implantation of piezoelectric materials in vivo has prompted encouraging results in repairing nerve injuries, bone formation and wound healing, which can be attributed to charge generation as a consequence of body movement and physiological stress on the piezoelectric material. Deformation of the piezoelectric scaffolds in vitro using mechanical or ultrasound agitation has also led to neurite extension, enhanced adhesion, differentiation and faster cellular migration. Even in the absence of deformation, piezoelectric scaffolds have exhibited favorable protein adsorption, cellular attachment and proliferation, possibly due to permanent polarization and surface charges of piezoelectric materials or transient deformation caused by the contraction and protrusion of the attached cells. Piezoelectric materials hold promise as the next generation of tissue engineering scaffolds.

Acknowledgements

The authors would like to thank support from DOD W81XWH-14-1-0482 and NSF DMR-1006510.

References

[1] P. Curie, J. Curie, Développement, par pression, de l'électricité polaire dans les cristaux hémièdres à faces inclinées, C.R. Acad. Sci. 91 (1880) 294–295.
[2] A.J.P. Martin, Tribo-electricity in wool and hair, Proc. Phys. Soc. 53 (1941) 186.
[3] R.C. Marshall, J. Gillespie, The keratin proteins of wool, horn and hoof from sheep, Austr. J. Biol. Sci. 30 (1977) 389–400.
[4] D.D. Wu, D.M. Irwin, Y.P. Zhang, Molecular evolution of the keratin associated protein gene family in mammals, role in the evolution of mammalian hair, BMC Evol. Biol. 8 (2008) 1471–2148.
[5] E. Menefee, Thermocurrent from alpha-helix disordering in keratin, in: M.M. Perlman (Ed.), Electrets, Charge Storage, and Transport in Dielectrics, Dielectrics and Insulation Division, Electrochemical Society, 1973, p. 661.
[6] M. Feughelman, D. Lyman, E. Menefee, B. Willis, The orientation of the α-helices in α-keratin fibres, Int. J. Biol. Macromol. 33 (2003) 149–152.
[7] D. Farrar, K. Ren, D. Cheng, S. Kim, W. Moon, W.L. Wilson, et al., Permanent polarity and piezoelectricity of electrospun α-helical poly(α-amino acid) fibers, Adv. Mater. 23 (2011) 3954–3958.
[8] A. Alparone, Response electric properties of α-helix polyglycines: a CAM-B3LYP DFT investigation, Chem. Phys. Lett. 563 (2013) 88–92.
[9] I. Yasuda, On the piezoelectric activity of bone, J. Jpn. Orthop. Surg. Soc. 28 (1954) 267–271.
[10] E. Fukada, I. Yasuda, On the piezoelectric effect of bone, J. Phys. Soc. Jpn. 12 (1957) 1158–1162.
[11] T. Hassenkam, G.E. Fantner, J.A. Cutroni, J.C. Weaver, D.E. Morse, P.K. Hansma, High-resolution AFM imaging of intact and fractured trabecular bone, Bone 35 (2004) 4–10.
[12] G.N. Ramachandran, G. Kartha, Structure of collagen, Nature 176 (1955) 593–595.
[13] K. Momeni, A. Asthana, A. Prasad, Y. Yap, R. Shahbazian-Yassar, Structural inhomogeneity and piezoelectric enhancement in ZnO nanobelts, Appl. Phys. A 109 (2012) 95–100.
[14] M. Minary-Jolandan, M.-F. Yu, Mechanical and electromechanical characterization of one-dimensional piezoelectric nanomaterials, in: G. Ciofani, A. Menciassi (Eds.), Piezoelectric Nanomaterials for Biomedical Applications, Springer Berlin Heidelberg, 2012, pp. 63–91.
[15] M. Minary-Jolandan, M.F. Yu, Nanoscale characterization of isolated individual type I collagen fibrils: polarization and piezoelectricity, Nanotechnology 20 (2009) 0957–4484.
[16] M. Minary-Jolandan, M.-F. Yu, Uncovering nanoscale electromechanical heterogeneity in the subfibrillar structure of collagen fibrils responsible for the piezoelectricity of bone, ACS Nano 3 (2009) 1859–1863.
[17] M.I. Kay, R.A. Young, A.S. Posner, Crystal structure of hydroxyapatite, Nature 204 (1964) 1050–1052.
[18] A. Gruverman, D. Wu, B.J. Rodriguez, S.V. Kalinin, S. Habelitz, High-resolution imaging of proteins in human teeth by scanning probe microscopy, Biochem. Biophys. Res. Commun. 352 (2007) 142–146.
[19] L. Calderín, M.J. Stott, A. Rubio, Electronic and crystallographic structure of apatites, Phys. Rev. B 67 (2003) 134106.
[20] S.B. Lang, S.A.M. Tofail, A.L. Kholkin, M. Wojtaś, M. Gregor, A.A. Gandhi, et al., Ferroelectric polarization in nanocrystalline hydroxyapatite thin films on silicon, Sci. Rep. 3 (2013).
[21] S.B. Lang, Pyroelectric effect in bone and tendon, Nature 212 (1966) 704–705.
[22] A.A. Marino, R.O. Becker, Piezoelectricity in hydrated frozen bone and tendon, Nature 253 (1975) 627–628.
[23] W.S. Williams, L. Breger, Piezoelectricity in tendon and bone, J. Biomech. 8 (1975) 407–413.
[24] A.R. Liboff, M.H. Shamos, Piezoelectric effect in dentin, J. Dent. Res. 50 (1971) 516.
[25] A.A. Marino, B.D. Gross, Piezoelectricity in cementum, dentine and bone, Arch. Oral Biol. 34 (1989) 507–509.
[26] M.H. Shamos, L.S. Lavine, Piezoelectricity as a fundamental property of biological tissues, Nature 213 (1967) 267–269.
[27] C.A. Bassett, R.J. Pawluk, Electrical behavior of cartilage during loading, Science (New York, NY) 178 (1972) 982–983.
[28] A.V. Shubnikov, I.S. Zheludev, V.P. Konstantinova, I.M. Silvestrova, Etude des Textures Piezoelectriques, 1958.
[29] E. Fukada, S. Sasaki, Piezoelectricity of α-chitin, J. Polym. Sci.: Polym. Phys. Ed. 13 (1975) 1845–1847.
[30] J. Duchesne, J. Depireux, A. Bertinchamps, N. Cornet, J.M. Van Der Kaa, Thermal and electrical properties of nucleic acids and proteins, Nature 188 (1960) 405–406.
[31] J. Wolff, Das gesetz der transformation der knochen, DMW – Deutsch. Med. Wochenschr. 19 (1892) 1222–1224.

[32] C.A.L. Bassett, Biologic significance of piezoelectricity, Calcif. Tissue Int. 1 (1967) 252–272.
[33] G.V.B. Cochran, Electromechanical characteristics of moist bone, 1966.
[34] J.C. Anderson, C. Eriksson, Electrical properties of wet collagen, Nature 218 (1968) 166–168.
[35] R.O. Becker, F.M. Brown, Photoelectric effects in human bone, Nature 206 (1965) 1325–1328.
[36] M.W. Johnson, D.A. Chakkalakal, R.A. Harper, J.L. Katz, Comparison of the electromechanical effects in wet and dry bone, J. Biomech. 13 (1980) 437–442.
[37] D. Gross, W.S. Williams, Streaming potential and the electromechanical response of physiologically-moist bone, J. Biomech. 15 (1982) 277–295.
[38] D. Pienkowski, S.R. Pollack, The origin of stress-generated potentials in fluid-saturated bone, J. Orthop. Res. 1 (1983) 30–41.
[39] R.C. Riddle, H.J. Donahue, From streaming-potentials to shear stress: 25 years of bone cell mechanotransduction, J. Orthop. Res. 27 (2009) 143–149.
[40] A.C. Ahn, A.J. Grodzinsky, Relevance of collagen piezoelectricity to "Wolff's Law": a critical review, Med. Eng. Phys. 31 (2009) 733–741.
[41] M.E. Mycielska, M.B. Djamgoz, Cellular mechanisms of direct-current electric field effects: galvanotaxis and metastatic disease, J. Cell Sci. 117 (2004) 1631–1639.
[42] R. Nuccitelli, Endogenous electric fields in embryos during development, regeneration and wound healing, Radiat. Prot. Dosimetry 106 (2003) 375–383.
[43] R. Nuccitelli, A role for endogenous electric fields in wound healing, Curr. Top. Dev. Biol. (2003) 1–26. Academic Press.
[44] C.D. McCaig, A.M. Rajnicek, B. Song, M. Zhao, Has electrical growth cone guidance found its potential?, Trends Neurosci 25 (2002) 354–359.
[45] S. Sundelacruz, M. Levin, D.L. Kaplan, Role of membrane potential in the regulation of cell proliferation and differentiation, Stem Cell Rev. 5 (2009) 231–246.
[46] D.A. McCormick, Chapter 12 – Membrane potential and action potential, in: J.H. Byrne, R. Heidelberger, M.N. Waxham (Eds.), From Molecules to Networks, third ed., Academic Press, Boston, 2014, pp. 351–376.
[47] L.F. Jaffe, M.-M. Poo, Neurites grow faster towards the cathode than the anode in a steady field, J. Exp. Zool. 209 (1979) 115–127.
[48] N. Patel, M.M. Poo, Orientation of neurite growth by extracellular electric fields, J. Neurosci. 2 (1982) 483–496.
[49] C.A.L. Bassett, R.J. Pawluk, R.O. Becker, Effects of electric currents on bone in vivo, Nature 204 (1964) 652–654.
[50] T. Kobayashi, S. Nakamura, K. Yamashita, Enhanced osteobonding by negative surface charges of electrically polarized hydroxyapatite, J. Biomed. Mater. Res. 57 (2001) 477–484.
[51] H.T. Nguyen, C. Wei, J.K. Chow, L. Nguy, H.K. Nguyen, C.E. Schmidt, Electric field stimulation through a substrate influences Schwann cell and extracellular matrix structure, J. Neural Eng. 10 (2013) 1741–2560.
[52] C.E. Schmidt, V. Shastri, E.J. Furnish, R. Langer, Electrical stimulation of neurite outgrowth and nerve regeneration, in: Biomedical Engineering Conference, 1998 Proceedings of the 17th Southern, IEEE, 1998, p. 117.
[53] M.P. Prabhakaran, L. Ghasemi-Mobarakeh, G. Jin, S. Ramakrishna, Electrospun conducting polymer nanofibers and electrical stimulation of nerve stem cells, J. Biosci. Bioeng. 112 (2011) 501–507.
[54] S.I. Jeong, I.D. Jun, M.J. Choi, Y.C. Nho, Y.M. Lee, H. Shin, Development of electroactive and elastic nanofibers that contain polyaniline and poly(L-lactide-co-ε-caprolactone) for the control of cell adhesion, Macromol. Biosci. 8 (2008) 627–637.
[55] C.E. Schmidt, V.R. Shastri, J.P. Vacanti, R. Langer, Stimulation of neurite outgrowth using an electrically conducting polymer, Proc. Natl. Acad. Sci. 94 (1997) 8948–8953.
[56] A. Kotwal, C.E. Schmidt, Electrical stimulation alters protein adsorption and nerve cell interactions with electrically conducting biomaterials, Biomaterials 22 (2001) 1055–1064.
[57] J.Y. Lee, C.A. Bashur, A.S. Goldstein, C.E. Schmidt, Polypyrrole-coated electrospun PLGA nanofibers for neural tissue applications, Biomaterials 30 (2009) 4325–4335.
[58] L. Ghasemi-Mobarakeh, M.P. Prabhakaran, M. Morshed, M.H. Nasr-Esfahani, S. Ramakrishna, Electrical stimulation of nerve cells using conductive nanofibrous scaffolds for nerve tissue engineering, Tissue Eng., Part A 15 (2009) 3605–3619.
[59] FDA, Premarket Approval, 1986.
[60] FDA, Premarket Approval, 1999.
[61] H. Zhuang, W. Wang, R.M. Seldes, A.D. Tahernia, H. Fan, C.T. Brighton, Electrical stimulation induces the level of TGF-β1 mRNA in osteoblastic cells by a mechanism involving calcium/calmodulin pathway, Biochem. Biophys. Res. Commun. 237 (1997) 225–229.
[62] M. Hartig, U. Joos, H.-P. Wiesmann, Capacitively coupled electric fields accelerate proliferation of osteoblast-like primary cells and increase bone extracellular matrix formation in vitro, Eur. Biophys. J. 29 (2000) 499–506.
[63] H.-P. Wiesmann, M. Hartig, U. Stratmann, U. Meyer, U. Joos, Electrical stimulation influences mineral formation of osteoblast-like cells in vitro. Biochimica et Biophysica Acta (BBA) - Molecular, Cell Res. 1538 (2001) 28–37.
[64] V. Cane, P. Botti, S. Soana, Pulsed magnetic fields improve osteoblast activity during the repair of an experimental osseous defect, J. Orthop. Res. 11 (1993) 664–670.
[65] C.H. Lohmann, Z. Schwartz, Y. Liu, H. Guerkov, D.D. Dean, B. Simon, et al., Pulsed electromagnetic field stimulation of MG63 osteoblast-like cells affects differentiation and local factor production, J. Orthop. Res. 18 (2000) 637–646.
[66] T. Bodamyali, B. Bhatt, F.J. Hughes, V.R. Winrow, J.M. Kanczler, B. Simon, et al., Pulsed electromagnetic fields simultaneously induce osteogenesis and upregulate transcription of bone morphogenetic proteins 2 and 4 in rat osteoblasts in vitro, Biochem. Biophys. Res. Commun. 250 (1998) 458–461.
[67] T. Takano-Yamamoto, M. Kawakami, M. Sakuda, Effect of a pulsing electromagnetic field on demineralized bone-matrix-induced bone formation in a bony defect in the premaxilla of rats, J. Dent. Res. 71 (1992) 1920–1925.
[68] W.H.-S. Chang, L.-T. Chen, J.-S. Sun, F.-H. Lin, Effect of pulse-burst electromagnetic field stimulation on osteoblast cell activities, Bioelectromagnetics 25 (2004) 457–465.
[69] E.K. Onuma, S.W. Hui, Electric field-directed cell shape changes, displacement, and cytoskeletal reorganization are calcium dependent, J. Cell Biol. 106 (1988) 2067–2075.
[70] K. Yamashita, N. Oikawa, T. Umegaki, Acceleration and deceleration of bone-like crystal growth on ceramic hydroxyapatite by electric poling, Chem. Mater. 8 (1996) 2697–2700.
[71] G. Shirane, K. Suzuki, A. Takeda, Phase transitions in solid solutions of $PbZrO_3$ and $PbTiO_3$ (II) X-ray study, J. Phys. Soc. Jpn. 7 (1952) 12–18.
[72] P.J. Larson, B.C. Towe, Miniature ultrasonically powered wireless nerve cuff stimulator, in: Neural Engineering (NER), 2011 5th International IEEE/EMBS Conference on 2011, pp. 265–268.
[73] J. Wen, M. Liu, Piezoelectric ceramic (PZT) modulates axonal guidance growth of rat cortical neurons via RhoA, Rac1, and Cdc42 pathways, J. Mol. Neurosci. 52 (2014) 323–330.
[74] J.M. Davis, D.A. Otto, D.E. Weil, L.D. Grant, The comparative developmental neurotoxicity of lead in humans and animals, Neurotoxicol. Teratol. 12 (1990) 215–229.
[75] M. Vigeh, K. Yokoyama, A. Shinohara, M. Afshinrokh, M. Yunesian, Early pregnancy blood lead levels and the risk of premature rupture of the membranes, Reprod. Toxicol. 30 (2010) 477–480.
[76] M. Ha, H.-J. Kwon, M.-H. Lim, Y.-K. Jee, Y.-C. Hong, J.-H. Leem, et al., Low blood levels of lead and mercury and symptoms of attention deficit hyperactivity in children: a report of the children's health and environment research (CHEER), NeuroToxicology 30 (2009) 31–36.
[77] R. Shukla, R.L. Bornschein, K.N. Dietrich, C.R. Buncher, O.G. Berger, P.B. Hammond, et al., Fetal and infant lead exposure: effects on growth in stature, Pediatrics 84 (1989) 604–612.
[78] W.P. Chen, H.L.W. Chan, F.C.H. Yiu, K.M.W. Ng, P.C.K. Liu, Water-induced degradation in lead zirconate titanate piezoelectric ceramics, Appl. Phys. Lett. 80 (2002) 3587–3589.
[79] J. Zhou, N.S. Xu, Z.L. Wang, Dissolving behavior and stability of ZnO wires in biofluids: a study on biodegradability and biocompatibility of ZnO nanostructures, Adv. Mater. 18 (2006) 2432–2435.
[80] H.W. Nesbitt, G.M. Bancroft, W.S. Fyfe, S.N. Karkhanis, A. Nishijima, S. Shin, Thermodynamic stability and kinetics of perovskite dissolution, Nature 289 (1981) 358–362.
[81] S.-W. Yu, S.-T. Kuo, W.-H. Tuan, Y.-Y. Tsai, S.-F. Wang, Cytotoxicity and degradation behavior of potassium sodium niobate piezoelectric ceramics, Ceram. Int. 38 (2012) 2845–2850.
[82] A. Bagchi, S.R.K. Meka, B.N. Rao, K. Chatterjee, Perovskite ceramic nanoparticles in polymer composites for augmenting bone tissue regeneration, Nanotechnology 25 (2014) 485101.
[83] W. Lin, Y. Xu, C.-C. Huang, Y. Ma, K. Shannon, D.-R. Chen, et al., Toxicity of nano- and micro-sized ZnO particles in human lung epithelial cells, J. Nanopart. Res. 11 (2009) 25–39.
[84] J.T. Seil, T.J. Webster, Decreased astroglial cell adhesion and proliferation on zinc oxide nanoparticle polyurethane composites, Int. J. Nanomedicine 3 (2008) 523–531.
[85] T. Amna, M.S. Hassan, F.A. Sheikh, H.K. Lee, K.S. Seo, D. Yoon, et al., Zinc oxide-doped poly(urethane) spider web nanofibrous scaffold via one-step electrospinning: a novel matrix for tissue engineering, Appl. Microbiol. Biotechnol. 97 (2013) 1725–1734.
[86] F. Baxter, I. Turner, C. Bowen, J. Gittings, J. Chaudhuri, An in vitro study of electrically active hydroxyapatite-barium titanate ceramics using Saos-2 cells, J. Mater. Sci.: Mater. Med. 20 (2009) 1697–1708.
[87] F. Jianqing, Y. Huipin, Z. Xingdong, Promotion of osteogenesis by a piezoelectric biological ceramic, Biomaterials 18 (1997) 1531–1534.
[88] Y. Zhang, L. Chen, J. Zeng, K. Zhou, D. Zhang, Aligned porous barium titanate/hydroxyapatite composites with high piezoelectric coefficients for bone tissue engineering, Mater. Sci. Eng., C 39 (2014) 143–149.
[89] G. Ciofani, S. Danti, D. D'Alessandro, S. Moscato, A. Menciassi, Assessing cytotoxicity of boron nitride nanotubes: interference with the MTT assay, Biochem. Biophys. Res. Commun. 394 (2010) 405–411.
[90] X. Chen, P. Wu, M. Rousseas, D. Okawa, Z. Gartner, A. Zettl, et al., Boron nitride nanotubes are noncytotoxic and can be functionalized for interaction with proteins and cells, J. Am. Chem. Soc. 131 (2009) 890–891.
[91] L. Horváth, A. Magrez, D. Golberg, C. Zhi, Y. Bando, R. Smajda, et al., In vitro investigation of the cellular toxicity of boron nitride nanotubes, ACS Nano 5 (2011) 3800–3810.
[92] G. Ciofani, S. Del Turco, A. Rocca, G. de Vito, V. Cappello, M. Yamaguchi, et al., Cytocompatibility evaluation of gum Arabic-coated ultra-pure boron nitride

nanotubes on human cells, Nanomedicine (London, England) 9 (2014) 773–788.
[93] J.B. Park, B.J. Kelly, G.H. Kenner, A.F. von Recum, M.F. Grether, W.W. Coffeen, Piezoelectric ceramic implants: in vivo results, J. Biomed. Mater. Res. 15 (1981) 103–110.
[94] G. Ciofani, L. Ricotti, C. Canale, D. D'Alessandro, S. Berrettini, B. Mazzolai, et al., Effects of barium titanate nanoparticles on proliferation and differentiation of rat mesenchymal stem cells, Colloids Surf., B 102 (2013) 312–320.
[95] Q. Wang, J. Yang, W. Zhang, R. Khoie, Y.M. Li, J.G. Zhu, et al., Manufacture and cytotoxicity of a lead-free piezoelectric ceramic as a bone substitute-consolidation of porous lithium sodium potassium niobate by cold isostatic pressing, Int. J. Oral Sci. 1 (2009) 99–104.
[96] G. Ciofani, S. Danti, D. D'Alessandro, L. Ricotti, S. Moscato, G. Bertoni, et al., Enhancement of neurite outgrowth in neuronal-like cells following boron nitride nanotube-mediated stimulation, ACS Nano 4 (2010) 6267–6277.
[97] H. Kawai, The piezoelectricity of poly(vinylidene fluoride), Jpn. J. Appl. Phys. 8 (1969) 975.
[98] F.S. Foster, K.A. Harasiewicz, M.D. Sherar, A history of medical and biological imaging with polyvinylidene fluoride (PVDF) transducers, IEEE Trans. Ultrason. Ferroelectr. Freq. Control 47 (2000) 1363–1371.
[99] X. Liu, X. Wang, H. Zhao, Y. Du, Myocardial cell pattern on piezoelectric nanofiber mats for energy harvesting, J. Phys: Conf. Ser. 557 (2014) 012057.
[100] K. Chelakara Satyanarayana, K. Bolton, Molecular dynamics simulations of α- to β-poly(vinylidene fluoride) phase change by stretching and poling, Polymer 53 (2012) 2927–2934.
[101] H. Ohigashi, K. Koga, M. Suzuki, T. Nakanishi, K. Kimura, N. Hashimoto, Piezoelectric and ferroelectric properties of P (VDF-TrFE) copolymers and their application to ultrasonic transducers, Ferroelectrics 60 (1984) 263–276.
[102] P. Aebischer, R.F. Valentini, P. Dario, C. Domenici, V. Guénard, S.R. Winn, et al., Piezoelectric nerve guidance channels enhance peripheral nerve regeneration, ASAIO J. 33 (1987) 457–458.
[103] E.G. Fine, R.F. Valentini, R. Bellamkonda, P. Aebischer, Improved nerve regeneration through piezoelectric vinylidenefluoride-trifluoroethylene copolymer guidance channels, Biomaterials 12 (1991) 775–780.
[104] R.F. Valentini, T.G. Vargo, J.A. Gardella Jr, P. Aebischer, Electrically charged polymeric substrates enhance nerve fibre outgrowth in vitro, Biomaterials 13 (1992) 183–190.
[105] N. Weber, Y.S. Lee, S. Shanmugasundaram, M. Jaffe, T.L. Arinzeh, Characterization and in vitro cytocompatibility of piezoelectric electrospun scaffolds, Acta Biomater. 6 (2010) 3550–3556.
[106] Y.-S. Lee, G. Collins, T. Livingston Arinzeh, Neurite extension of primary neurons on electrospun piezoelectric scaffolds, Acta Biomater. 7 (2011) 3877–3886.
[107] Y.S. Lee, T.L. Arinzeh, The influence of piezoelectric scaffolds on neural differentiation of human neural stem/progenitor cells, Tissue Eng., Part A 18 (2012) 2063–2072.
[108] S.M. Damaraju, S. Wu, M. Jaffe, T.L. Arinzeh, Structural changes in PVDF fibers due to electrospinning and its effect on biological function, Biomed. Mater. 8 (2013) 045007.
[109] H.F. Guo, Z.S. Li, S.W. Dong, W.J. Chen, L. Deng, Y.F. Wang, et al., Piezoelectric PU/PVDF electrospun scaffolds for wound healing applications, Colloids Surf. B Biointerfaces 96 (2012) 29–36.
[110] N. Royo-Gascon, M. Wininger, J.I. Scheinbeim, B.L. Firestein, W. Craelius, Piezoelectric substrates promote neurite growth in rat spinal cord neurons, Ann. Biomed. Eng. 41 (2013) 112–122.
[111] C. Ribeiro, J.A. Panadero, V. Sencadas, S. Lanceros-Méndez, M.N. Tamaño, D. Moratal, et al., Fibronectin adsorption and cell response on electroactive poly(vinylidene fluoride) films, Biomed. Mater. 7 (2012) 035004.
[112] C. Ribeiro, J. Pärssinen, V. Sencadas, V. Correia, S. Miettinen, V.P. Hytönen, et al., Dynamic piezoelectric stimulation enhances osteogenic differentiation of human adipose stem cells, J. Biomed. Mater. Res., Part A 103 (2015) 2172–2175.
[113] J. Pärssinen, H. Hammarén, R. Rahikainen, V. Sencadas, C. Ribeiro, S. Vanhatupa, et al., Enhancement of adhesion and promotion of osteogenic differentiation of human adipose stem cells by poled electroactive poly(vinylidene fluoride), J. Biomed. Mater. Res., Part A 103 (2015) 919–928.
[114] H. Tamai, K. Igaki, E. Kyo, K. Kosuga, A. Kawashima, S. Matsui, et al., Initial and 6-month results of biodegradable poly-l-lactic acid coronary stents in humans, Circulation 102 (2000) 399–404.
[115] E. Fukada, Bioelectrets and biopiezoelectricity, IEEE Trans. Electr. Insul. 27 (1992) 813–819.
[116] J. Kobayashi, T. Asahi, M. Ichiki, A. Oikawa, H. Suzuki, T. Watanabe, et al., Structural and optical properties of poly lactic acids, J. Appl. Phys. 77 (1995) 2957–2973.
[117] E. Fukada, Piezoelectric properties of poly-L-lactic acid, Rep. Prog. Polym. Phys. Jpn. 34 (1991) 269–272.
[118] Y. Ikada, Y. Shikinami, Y. Hara, M. Tagawa, E. Fukada, Enhancement of bone formation by drawn poly(L-lactide), J. Biomed. Mater. Res. 30 (1996) 553–558.
[119] FDA, 510(k) Summary, 2001.
[120] FDA, 510(k) Summary, 2008.
[121] F. Yang, R. Murugan, S. Ramakrishna, X. Wang, Y.X. Ma, S. Wang, Fabrication of nano-structured porous PLLA scaffold intended for nerve tissue engineering, Biomaterials 25 (2004) 1891–1900.
[122] F. Yang, R. Murugan, S. Wang, S. Ramakrishna, Electrospinning of nano/micro scale poly(L-lactic acid) aligned fibers and their potential in neural tissue engineering, Biomaterials 26 (2005) 2603–2610.
[123] M.P. Prabhakaran, J. Venugopal, S. Ramakrishna, Electrospun nanostructured scaffolds for bone tissue engineering, Acta Biomater. 5 (2009) 2884–2893.
[124] L. Jia, M.P. Prabhakaran, X. Qin, S. Ramakrishna, Stem cell differentiation on electrospun nanofibrous substrates for vascular tissue engineering, Mater. Sci. Eng., C 33 (2013) 4640–4650.
[125] N. Barroca, P.M. Vilarinho, A.L. Daniel-da-Silva, A. Wu, M.H. Fernandes, A. Gruverman, Protein adsorption on piezoelectric poly(L-lactic) acid thin films by scanning probe microscopy, Appl. Phys. Lett. 98 (2011) 133705.
[126] M. Minary-Jolandan, M.-F. Yu, Shear piezoelectricity in bone at the nanoscale, Appl. Phys. Lett. 97 (2010) 153127.
[127] T. Shrout, S. Zhang, Lead-free piezoelectric ceramics: alternatives for PZT?, J Electroceram. 19 (2007) 113–126.
[128] J.A. Christman, R.R. Woolcott, A.I. Kingon, R.J. Nemanich, Piezoelectric measurements with atomic force microscopy, Appl. Phys. Lett. 73 (1998) 3851–3853.
[129] D. Berlincourt, H. Jaffe, Elastic and piezoelectric coefficients of single-crystal barium titanate, Phys. Rev. 111 (1958) 143–148.
[130] C. Ying, S.W. Jim, Synthesis of Boron Nitride Nanotubes Using a Ball-Milling and Annealing Method. Nanoengineering of Structural, Functional and Smart Materials, CRC Press, 2005.
[131] K. Tashiro, M. Kobayashi, H. Tadokoro, E. Fukada, Calculation of elastic and piezoelectric constants of polymer crystals by a point charge model: application to poly(vinylidene fluoride) form I, Macromolecules 13 (1980) 691–698.
[132] P. Sharma, D. Wu, S. Poddar, T.J. Reece, S. Ducharme, A. Gruverman, Orientational imaging in polar polymers by piezoresponse force microscopy, J. Appl. Phys. 110 (2011) 052010.
[133] T. Ochiai, E. Fukada, Electromechanical properties of poly-L-lactic acid, Jpn. J. Appl. Phys. 37 (1998) 3374.